

# Excitation energy shift and size difference of low-energy levels in $p$ -shell $\Lambda$ hypernuclei

Yoshiko Kanada-En'yo

Department of Physics, Kyoto University, Kyoto 606-8502, Japan



(Received 11 September 2017; published 23 February 2018)

Structures of low-lying  $0s$ -orbit  $\Lambda$  states in  $p$ -shell  $\Lambda$  hypernuclei ( ${}^A_\Lambda Z$ ) are investigated by applying microscopic cluster models for nuclear structure and a single-channel folding potential model for a  $\Lambda$  particle. For  $A > 10$  systems, the size reduction of core nuclei is small, and the core polarization effect is regarded as a higher-order perturbation in the  $\Lambda$  binding. The present calculation qualitatively describes the systematic trend of experimental data for excitation energy change from  ${}^{A-1}Z$  to  ${}^A_\Lambda Z$ , in  $A > 10$  systems. The energy change shows a clear correlation with the nuclear size difference between the ground and excited states. In  ${}^7_\Lambda\text{Li}$  and  ${}^9_\Lambda\text{Be}$ , the significant shrinkage of cluster structures occurs consistently with the prediction of other calculations.

DOI: [10.1103/PhysRevC.97.024330](https://doi.org/10.1103/PhysRevC.97.024330)

## I. INTRODUCTION

Owing to high-resolution  $\gamma$ -ray measurement experiments, spectra of low-lying states of various  $p$ -shell  $\Lambda$  hypernuclei have been revealed [1–3]. Measured energy spectra and electromagnetic transitions are useful information to know properties of  $\Lambda$ -nucleon ( $\Lambda$ - $N$ ) interactions and also helpful to investigate impurity effects of a  $\Lambda$  particle on nuclear systems. In order to theoretically study structures of  $p$ -shell  $\Lambda$  hypernuclei, various calculations have been performed with cluster models [4–20], shell models [21–26], mean-field and beyond-mean-field models [27–36], hyperantisymmetrized molecular dynamics (HAMD) model [37–41], no-core shell model [42], and so on.

Since a  $\Lambda$  particle is free from Pauli blocking and  $\Lambda$ - $N$  interactions are weaker than  $N$ - $N$  interactions, the  $\Lambda$  spin degree of freedom in  $\Lambda$  hypernuclei more or less weakly couples with core nuclei in general. Therefore, the  $\Lambda$  particle in  $\Lambda$  hypernuclei can be regarded as an impurity of the nuclear system. Indeed, there are many theoretical works discussing  $\Lambda$  impurity effects of on nuclear structures such as shrinkage effects on cluster structures [4,5,7–13,38,39,43–45] and effects on nuclear deformations [29–32,37,40,46,47]. One of the famous phenomena is the shrinkage of  ${}^7_\Lambda\text{Li}$ , which has been theoretically predicted [4,5] and later evidenced experimentally through the  $E2$  transition strength measurement [48]. The dynamical effects of  $\Lambda$  on nuclear structures can be significant in the case that core nuclei are fragile systems such as weakly bound systems and shape softness (or coexistence) ones. However, except for such cases, dynamical change of nuclear structure (the core polarization) is expected to be minor in general because of the weaker  $\Lambda$ - $N$  interactions and no Pauli blocking. In this context, there might be a chance to probe original properties of core nuclear structures by a  $\Lambda$  particle perturbatively appended to the nuclear system.

Let me focus on energy spectra of  $p$ -shell  $\Lambda$  hypernuclei. The low-energy levels are understood as core-excited states with a  $0s$  orbit  $\Lambda$  [ $(0s)_\Lambda$  states]. When the  $\Lambda$  particle is considered to be an impurity giving a perturbation to the core nuclear system, the first-order perturbation on the energy spectra, that

is, change of excitation energies by the  $\Lambda$  particle, comes from structure difference between the ground and excited states through the  $\Lambda$ - $N$  interactions, whereas dynamical structure change gives second-order perturbation effects on the energy spectra. For excited states with structures much different from that of the ground state, the  $\Lambda$  particle can give significant effect on energy spectra as discussed by Isaka *et al.* for Be isotopes [38,39]. In this concern, it is meaningful to look at excitation energy shifts, that is, excitation energy changes from  ${}^{A-1}Z$  to  ${}^A_\Lambda Z$ , in available data. For simplicity, the  $\Lambda$  intrinsic spin degree of freedom is ignored because spin dependence of the  $\Lambda$ - $N$  interactions is weak. In the observed energy spectra of  ${}^{10}_\Lambda\text{B}$ ,  ${}^{11}_\Lambda\text{B}$ ,  ${}^{11}_\Lambda\text{C}$ , and  ${}^{12}_\Lambda\text{C}$  systems, one can see that the excitation energies ( $E_x$ ) for  ${}^{10}\text{B}(3^+)$ ,  ${}^{11}\text{B}(1/2^-, 3/2^-)$ ,  ${}^{11}\text{C}(1/2^-, 3/2^-)$ , and  ${}^{12}\text{C}(2^+)$  are significantly raised by the  $\Lambda$  particle in  ${}^A_\Lambda Z$  systems compared with those in  ${}^{A-1}Z$  systems. On the other hand, the situation is opposite in  ${}^6\text{Li}$ - ${}^7\text{Li}$  systems. the  $E_x(3^+)$  is decreased by the  $\Lambda$  particle. To systematically comprehend the energy spectra of  $p$ -shell  $\Lambda$  hypernuclei, it is worth examining the excitation energy shifts and their link with the structure difference between the ground and excited states.

Precise data of spectroscopy in various  $\Lambda$  hypernuclei are becoming available and they provide fascinating physics in nuclear many-body systems consisting of protons, neutrons, and  $\Lambda$ s. Sophisticated calculations have been achieved mainly in light nuclei and greatly contributed to the progress of physics of hypernuclei. Nevertheless, systematic studies for energy spectra of hypernuclei in a wide mass-number region are still limited compared with those for ordinary nuclei, for which various structure models have been developed and used for intensive and extensive studies. It is time to extend application of such structure models developed for ordinary nuclei to hypernuclei. To this end, it might be helpful to propose a handy and economical treatment of a  $\Lambda$  particle and core polarization in  $\Lambda$  hypernuclei that can be applied to general structure models.

The first aim in this paper is to investigate energy spectra of low-lying  $(0s)_\Lambda$  states in  $p$ -shell  $\Lambda$  hypernuclei. Particular

attention is paid to the excitation energy shifts by the  $\Lambda$  and their link with structures of core nuclei. The second aim is to propose a handy treatment of the  $\Lambda$  particle in  $\Lambda$  hypernuclei and to check its phenomenological applicability. To describe detailed structures of the ground and excited states of core nuclei, The generator coordinate method (GCM) [49,50] of microscopic  $\alpha + d$ ,  $2\alpha$ , and  $2\alpha + d$  cluster models is applied for  ${}^6\text{Li}$ ,  ${}^8\text{Be}$ , and  ${}^{10}\text{B}$ , respectively, and that of extended  $2\alpha + t$  and  $3\alpha$  cluster models with the cluster breaking for  ${}^{11}\text{B}$ ,  ${}^{11}\text{C}$ , and  ${}^{12}\text{C}$ . For description of  $(0s)_\Lambda$  states in  $\Lambda$  hypernuclei, a single  $S$ -wave channel calculation with a folding potential model is performed. Namely, the  $\Lambda$ -nucleus potentials are constructed by folding  $\Lambda$ - $N$  interactions with the nuclear density calculated by the microscopic cluster models. As a core polarization effect, the core size reduction is taken into account in a simple way.

This paper is organized as follows. In the next section, formalism of the present model is described. The adopted effective  $N$ - $N$  and  $\Lambda$ - $N$  interactions are explained in Sec. III. The results are shown in Sec. IV, and discussions are given in Sec. V. Finally, the paper is summarized in Sec. VI.

## II. FORMULATION

### A. Microscopic cluster model for core nuclei

Structures of core nuclei are calculated by the microscopic cluster models with the GCM using the Brink-Bloch cluster wave functions [51]. In the cluster GCM calculations, the microscopic  $\alpha + d$ ,  $2\alpha$ , and  $2\alpha + d$ ,  $2\alpha + t(h)$ , and  $3\alpha$  wave functions are superposed for  ${}^6\text{Li}$ ,  ${}^8\text{Be}$ ,  ${}^{10}\text{B}$ ,  ${}^{11}\text{B}(\text{C})$ , and  ${}^{12}\text{C}$ , respectively.

For a system consisting of  $C_1, \dots, C_k$  clusters ( $k$  is the number of clusters), the Brink-Bloch cluster wave function is given as

$$\begin{aligned} \Phi_{\text{BB}}(\mathbf{S}_1, \dots, \mathbf{S}_k; \mathbf{r}_1\sigma_1, \dots, \mathbf{r}_A\sigma_A) \\ = \mathcal{A}[\phi_{C_1}(\mathbf{S}_1; \mathbf{r}_1\sigma_1, \dots, \mathbf{r}_{A_1}\sigma_{A_1}) \\ \cdots \phi_{C_k}(\mathbf{S}_k; \mathbf{r}_{A-A_k}\sigma_{A-A_k}, \dots, \mathbf{r}_{A_k}\sigma_{A_k})], \end{aligned} \quad (1)$$

where  $\mathbf{S}_j$  indicates the position parameter of the  $C_j$  cluster,  $\mathbf{r}_i$  and  $\sigma_i$  indicate the coordinate and spin-isospin configuration of the  $i$ th nucleon,  $\mathcal{A}$  is the antisymmetrizer of all nucleons,  $A$  is the mass number, and  $A_j$  is the mass number of the  $C_j$  cluster. The  $A_j$ -nucleon wave function  $\phi_{C_j}$  for the  $C_j$  cluster is written by the  $(0s)^{A_j}$  harmonic oscillator shell model wave function with the center shifted to the position  $\mathbf{S}_j$ . The intrinsic spin configurations of  $d$ ,  $t(h)$ , and  $\alpha$  clusters are  $S = 1$ ,  $1/2$ , and  $0$  states, respectively. The width parameter  $\nu = 1/(2b^2)$  ( $b$  is the size parameter) of the harmonic oscillator is set to be a common value so that the center of mass (cm) motion can be removed exactly. In the present work, parameter  $\nu = 0.235 \text{ fm}^{-2}$ , which reasonably reproduces the ground-state sizes of  $p$ -shell nuclei, is adopted as used in Ref. [55]. The Brink-Bloch cluster wave function is a fully microscopic  $A$ -nucleon wave function, in which the degrees of freedom and antisymmetrization of  $A$  nucleons are taken into account, differently from nonmicroscopic cluster models

(simple  $k$ -body potential models) and such semimicroscopic cluster models as the orthogonal condition model (OCM) [52].

To take into account intercluster motion, the GCM is performed with respect to the cluster center parameters  $\mathbf{S}_j$ . Namely, the GCM wave function  $\Psi(J_n^\pi)$  for the  $J_n^\pi$  state is expressed by linear combination of the spin-parity projected Brink-Bloch wave functions with various configurations of  $\mathbf{S}_j$  as

$$\Psi(J_n^\pi) = \sum_{\mathbf{S}_1, \dots, \mathbf{S}_k} \sum_K c_{\mathbf{S}_1, \dots, \mathbf{S}_k, K}^{J_n^\pi} P_{MK}^{J_n^\pi} \Phi_{\text{BB}}(\mathbf{S}_1, \dots, \mathbf{S}_k), \quad (2)$$

where  $P_{MK}^{J_n^\pi}$  is the spin-parity projection operator. The coefficients  $c_{\mathbf{S}_1, \dots, \mathbf{S}_k, K}^{J_n^\pi}$  are determined by diagonalization of the Hamiltonian and norm matrices. In the present calculation, for two-cluster systems of  $\alpha + d$  and  $2\alpha$ ,  $\mathbf{S}_k$  is chosen to be  $\mathbf{S}_1 - \mathbf{S}_2 = (0, 0, d)$  with  $d = \{1, 2, \dots, 15 \text{ fm}\}$ . For three-cluster systems of  $2\alpha + d$ ,  $2\alpha + t(h)$ ,  $3\alpha$ ,  $\mathbf{S}_k$  is chosen to be

$$\mathbf{S}_1 - \mathbf{S}_2 = (0, 0, d), \quad (3)$$

$$\mathbf{S}_3 - \frac{A_2\mathbf{S}_1 + A_1\mathbf{S}_2}{A_1 + A_2} = (r \sin \theta, 0, r \cos \theta), \quad (4)$$

with  $d = \{1.2, 2.4, \dots, 4.2 \text{ fm}\}$ ,  $r = \{0.5, 1.5, \dots, 4.5 \text{ fm}\}$ ,  $\theta = \{0, \pi/8, \dots, \pi/2\}$ .

In a long history of structure study of  ${}^8\text{Be}$  and  ${}^{12}\text{C}$ , the  $2\alpha$  and  $3\alpha$  GCM calculations have been performed in many works since the 1970s (see Refs. [53,54] and references therein), and successfully described cluster structures except for the ground state of  ${}^{12}\text{C}$ . For the ground state of  ${}^{12}\text{C}$ , the traditional  $3\alpha$  models are not sufficient because the cluster breaking component, in particular, the  $p_{3/2}$ -closed configuration is significantly mixed in it, and therefore, they usually fail to reproduce the  $0_1^+ - 2_1^+$  energy spacing and  $B(E2; 2_1^+ \rightarrow 0_1^+)$ . In order to take into account the cluster breaking component, Suhara and the author have proposed an extended  $3\alpha$  cluster model by adding the  $p_{3/2}$ -closed configuration in the  $3\alpha$  GCM calculation, which is called the  $3\alpha + p_{3/2}$  model [55]. In the present calculation of  ${}^{12}\text{C}$ , the  $3\alpha + p_{3/2}$  model is adopted. Also for  ${}^{11}\text{B}$ , a similar model of the  $2\alpha + t + p_{3/2}$  model is applied by adding the  $(p_{3/2})_\pi^3 (p_{3/2})_\alpha^4$  configuration to the  $2\alpha + t$  cluster wave functions in the GCM calculation [for  ${}^{11}\text{C}$ , the  $2\alpha + h + p_{3/2}$  model with the  $(p_{3/2})_\pi^4 (p_{3/2})_\alpha^3$  configuration to the  $2\alpha + h$  wave functions].

The nuclear density  $\rho_N(r)$  in the core nuclei is calculated for the obtained GCM wave function  $\Psi(J_n^\pi)$ . The  $\rho_N(r)$  is the  $r$ -dependent spherical density of the  $J_n^\pi$  state after extraction of the cm motion.

### B. Hamiltonian of nuclear part

Hamiltonian of the nuclear part consists of the kinetic term, effective nuclear interactions, and Coulomb interactions as follows:

$$H_N = T + V_N^{(c)} + V_N^{(\text{so})} + V_{\text{coul}}, \quad (5)$$

$$T = \sum_i^A \frac{1}{2m_N} p_i^2 - T_G, \quad (6)$$

$$V_N^{(c)} = \sum_{i < j}^A v_{NN}^{(c)}(i, j), \quad (7)$$

$$V_N^{(so)} = \sum_{i < j}^A v_{NN}^{(so)}(i, j), \quad (8)$$

$$V_{\text{coul}} = \sum_{i < j}^Z v_{\text{coul}}(r_{ij}), \quad (9)$$

where  $T_G$  is the kinetic term of the cm motion, and  $v_{NN}^{(c)}(i, j)$  and  $v_{NN}^{(so)}(i, j)$  are the effective  $N$ - $N$  central and spin-orbit interactions. The energy  $E_N$  of the core nucleus is given as  $E_N = \langle \Psi(J_n^\pi) | H_N | \Psi(J_n^\pi) \rangle$  (the nuclear energy). In the GCM calculation, the coefficients  $c_{S_1, \dots, S_k, K}^{J_n^\pi}$  in (2) are determined so as to minimize  $E_N$ .

### C. Hamiltonian and folding potential of $\Lambda$ -nucleus system

$(0s)_\Lambda$  states of  $\Lambda$  hypernuclei are calculated with a folding potential model by solving the following single  $S$ -wave channel problem within local density approximations,

$$H_\Lambda = T_\Lambda + U_\Lambda, \quad (10)$$

$$T_\Lambda = \frac{1}{2\mu_\Lambda} \mathbf{p}^2, \quad (11)$$

$$\mu_\Lambda = \frac{(A-1)m_N m_\Lambda}{(A-1)m_N + m_\Lambda}, \quad (12)$$

$$U_\Lambda(\mathbf{r}, \mathbf{r}') = U_\Lambda^D(\mathbf{r}) + |\mathbf{r}| U_\Lambda^{\text{EX}}(\mathbf{r}, \mathbf{r}') |\mathbf{r}'|, \quad (13)$$

$$U_\Lambda^D(\mathbf{r}) = \int \mathbf{r}'' \rho_N(\mathbf{r}'') v_{\Lambda N}^D(k_f; |\mathbf{r} - \mathbf{r}''|), \quad (14)$$

$$U_\Lambda^{\text{EX}}(\mathbf{r}, \mathbf{r}') = \rho_N(\mathbf{r}, \mathbf{r}') v_{\Lambda N}^{\text{EX}}(k_f; |\mathbf{r} - \mathbf{r}'|), \quad (15)$$

$$v_{\Lambda N}^D(k_f; r) = \frac{1}{2} [V_{\Lambda N}^e(k_f; r) + V_{\Lambda N}^o(k_f; r)], \quad (16)$$

$$v_{\Lambda N}^{\text{EX}}(k_f; r) = \frac{1}{2} [V_{\Lambda N}^e(k_f; r) - V_{\Lambda N}^o(k_f; r)], \quad (17)$$

where  $\mathbf{r}$ ,  $\mathbf{r}'$ , and  $\mathbf{p}$  are defined with respect to the relative coordinate of the  $\Lambda$  from the cm of the core nucleus.  $V_{\Lambda N}^e(k_f; r)$  and  $V_{\Lambda N}^o(k_f; r)$  are the even and odd parts of the effective  $\Lambda$ - $N$  central interactions, respectively, where  $k_f$  is the parameter for density dependence of the effective  $\Lambda$ - $N$  interactions.

The nuclear density matrix  $\rho_N(\mathbf{r}, \mathbf{r}')$  in the exchange potential  $U_\Lambda^{\text{EX}}(\mathbf{r}, \mathbf{r}')$  is approximated with the density matrix expansion (DME) using the LDA [58],

$$\rho_N(\mathbf{r}, \mathbf{r}') \sim \rho_N^{\text{DME}}(\mathbf{r}, \mathbf{r}'), \quad (18)$$

$$\rho_N^{\text{DME}}(\mathbf{r}, \mathbf{r}') = \rho_N^{\text{LDA}}(\mathbf{r}, \mathbf{r}') \left( \frac{3}{k_f^{\text{LDA}} |\mathbf{r} - \mathbf{r}'|} \right) j_1(k_f^{\text{LDA}} |\mathbf{r} - \mathbf{r}'|), \quad (19)$$

$$\rho_N^{\text{LDA}}(\mathbf{r}, \mathbf{r}') = \rho_N \left( \frac{\mathbf{r} + \mathbf{r}'}{2} \right), \quad (20)$$

$$k_f^{\text{LDA}} = \left[ \frac{3\pi^2}{2} \rho_N^{\text{LDA}}(\mathbf{r}, \mathbf{r}') \right]^{1/3}. \quad (21)$$

To see ambiguity of choice of local density and Fermi momentum in the DME approximation, the second choice (LDA2) is also adopted,

$$\rho_N^{\text{LDA2}}(\mathbf{r}, \mathbf{r}') = \frac{1}{2} [\rho_N(\mathbf{r}) + \rho_N(\mathbf{r}')], \quad (22)$$

$$k_f^{\text{LDA2}} = \left[ \frac{3\pi^2}{2} \rho_N^{\text{LDA2}}(\mathbf{r}, \mathbf{r}') \right]^{1/3}, \quad (23)$$

and found that the first and the second choices give qualitatively similar results. In this paper, the DME approximation in the first choice is used for the exchange folding potential  $U_\Lambda^{\text{EX}}(\mathbf{r}, \mathbf{r}')$ .

For a given nuclear density  $\rho_N(r)$ , the  $\Lambda$ -core wave function  $\phi_\Lambda(r)$  and energy  $E_\Lambda = \langle \phi_\Lambda | H_\Lambda | \phi_\Lambda \rangle$  are calculated by solving the one-body potential problem with the Gaussian expansion method [59,60]. The rms radius ( $r_\Lambda$ ) measured from the core nucleus and the averaged nuclear density ( $\langle \rho_N \rangle_\Lambda$ ) for the  $\Lambda$  distribution are calculated with the obtained  $\Lambda$ -core wave function  $\phi_\Lambda(r)$ ,

$$r_\Lambda = \sqrt{\int \phi_\Lambda^*(r) \phi_\Lambda(r) r^2 dr}, \quad (24)$$

$$\langle \rho_N \rangle_\Lambda = \int \phi_\Lambda^*(r) \phi_\Lambda(r) \rho_N(r) dr. \quad (25)$$

### D. Core polarization effect

The core polarization, which is the structure change of core nuclei caused by the impurity  $\Lambda$  in  $\Lambda$  hypernuclei, is taken into account as follows. In the present folding potential model, the  $\Lambda$  binding reflects the core nuclear structure only through the nuclear density  $\rho_N(r)$ . When the  $0s$ -orbit  $\Lambda$  particle is regarded as an impurity of the nuclear system, the  $\Lambda$ - $N$  interactions may act as an additional attraction to the nuclear system and make the nuclear size slightly small. To simulate the nuclear structure change induced by the  $0s$ -orbit  $\Lambda$ , artificial nuclear interactions is added by slightly enhancing the central part by hand and perform the GCM calculation of the nuclear system for the modified Hamiltonian,

$$H_N + \Delta H(\epsilon) = T + (1 + \epsilon) V_N^{(c)} + V_N^{(so)} + V_{\text{coul}}, \quad (26)$$

with the additional term  $\Delta H(\epsilon) = \epsilon V_N^{(c)}$ , where  $\epsilon$  is the enhancement factor and taken to be  $\epsilon \geq 0$ . For the GCM wave function  $\Phi(\epsilon; J_n^\pi)$  of the  $J_n^\pi$  state obtained with  $H_N + \Delta H(\epsilon)$ , the nuclear energy

$$E_N(\epsilon) = \langle \Phi(\epsilon; J_n^\pi) | H_N | \Phi(\epsilon; J_n^\pi) \rangle \quad (27)$$

and the nuclear density  $\rho_N(\epsilon; r)$  are calculated. Note that the nuclear energy  $E_N(\epsilon)$  is calculated for the original Hamiltonian  $H_N$  without the additional term, and the  $\epsilon$  dependence of  $E_N(\epsilon)$  comes from the  $\epsilon$  dependence of the wave function  $\Phi(\epsilon; J_n^\pi)$ . Then, the  $\Lambda$ -wave function  $[\phi_\Lambda(\epsilon; r)]$  and energy  $[E_\Lambda(\epsilon)]$  for the obtained  $\epsilon$ -dependent nuclear density  $\rho_N(\epsilon; r)$  are calculated. Finally, the optimum  $\epsilon$  value is chosen so as to minimize the energy of the total system,

$$E(\epsilon) = E_N(\epsilon) + E_\Lambda(\epsilon), \quad (28)$$

$$\frac{\delta E(\epsilon)}{\delta \epsilon} = 0. \quad (29)$$

The  $\Lambda$  binding energy ( $B_\Lambda$ ) is calculated as  $B_\Lambda = -[E(\epsilon) - E_N^{\text{up}}]$  for the optimized  $\epsilon$  value, where  $E_N^{\text{up}} = E_N(\epsilon = 0)$  is the unperturbative nuclear energy without the  $\Lambda$  particle.

The GCM coefficients for the fixed basis cluster wave functions are varied corresponding to the inert cluster ansatz. In this assumption, the enhancement of the effective central nuclear interactions acts like an enhancement of the intercluster potentials.

### III. EFFECTIVE INTERACTIONS

#### A. Effective nuclear interactions

The effective two-body nuclear interactions used in the present calculation are the finite-range central interactions of the Volkov No. 2 parametrization [61] and the spin-orbit interactions of the G3RS parametrization [62],

$$v_{NN}^{(c)}(1,2) = V_{NN}^{(c)}(r_{12})(w + bP_\sigma - hP_\tau - mP_\sigma P_\tau), \quad (30)$$

$$V_{NN}^{(c)}(r) = v_1 \exp\left[-\left(\frac{r}{a_1}\right)^2\right] + v_2 \exp\left[-\left(\frac{r}{a_2}\right)^2\right], \quad (31)$$

$$v_1 = -60.65 \text{ MeV}, v_2 = 61.14 \text{ MeV}, \quad (32)$$

$$a_1 = 1.80 \text{ fm}, a_2 = 1.01 \text{ fm}, \quad (33)$$

$$v_{NN}^{(\text{so})}(1,2) = V_{NN}^{(\text{so})}(r) \frac{1 + P_\sigma}{2} \frac{1 + P_\sigma P_\tau}{2} (\mathbf{I}_{12} \cdot \mathbf{s}_{12}), \quad (34)$$

$$V_{NN}^{(\text{so})}(r) = u_1 \exp\left[-\left(\frac{r}{b_1}\right)^2\right] + u_2 \exp\left[-\left(\frac{r}{b_2}\right)^2\right], \quad (35)$$

$$b_1 = 0.60 \text{ fm}, b_2 = 0.447 \text{ fm}, \quad (36)$$

where  $P_\sigma$  ( $P_\tau$ ) is the spin(isospin) exchange operator,  $r_{12}$  is the relative distance  $r_{12} = |\mathbf{r}_{12}|$  for the relative coordinate  $\mathbf{r}_{12} = \mathbf{r}_1 - \mathbf{r}_2$ ,  $\mathbf{I}_{12}$  is the angular momentum for  $\mathbf{r}_{12}$ , and  $\mathbf{s}_{12}$  is the sum of nucleon spins  $\mathbf{s}_{12} = \mathbf{s}_1 + \mathbf{s}_2$ .

As for the values of parameters,  $w = 0.40$ ,  $m = 0.60$ , and  $b = h = 0.125$  for the central interactions, and  $u_1 = -u_2 = 1600 \text{ MeV}$  for the spin-orbit interactions are used. These parameters reproduce the deuteron binding energy, the  $\alpha$ - $\alpha$  scattering phase shift, and properties of the ground and excited states of  $^{12}\text{C}$  [55,63,64]. For  $^6\text{Li}$ , modified values  $w = 0.43$ ,  $m = 0.57$ ,  $b = h = 0.125$ , and  $u_1 = -u_2 = 1200 \text{ MeV}$  are used to reproduce the  $^6\text{Li}(1_1^+)$  and  $^6\text{Li}(3_1^+)$  energies relative to the  $\alpha + d$  threshold energy. Note that this modification gives no effect on  $s$ -shell nuclei,  $d$ ,  $t$ ,  $h$ , and  $\alpha$ .

#### B. Effective $\Lambda$ -nucleon interactions

For the effective  $\Lambda$ - $N$  central interactions,  $G$ -matrix interactions derived from  $\Lambda$ - $N$  interactions of the one-boson-exchange model, which is denoted as the  $\Lambda NG$  interactions [56,57], are used. In this paper, the central part of the  $\Lambda NG$

TABLE I. Parameters of the  $\Lambda NG$  interactions of ESC08a from Table II of Ref. [56].

|                | $i = 1$ | $i = 2$ | $i = 3$ |
|----------------|---------|---------|---------|
| $c_{0,i}^{1E}$ | -3144   | 368.0   | -1.467  |
| $c_{1,i}^{1E}$ | 6411    | -984.4  | 0       |
| $c_{2,i}^{1E}$ | -2478   | 394.5   | 0       |
| $c_{0,i}^{3E}$ | -2734   | 316.8   | -1.044  |
| $c_{1,i}^{3E}$ | 5827    | -901.6  | 0       |
| $c_{2,i}^{3E}$ | -2404   | 395.8   | 0       |
| $c_{0,i}^{1O}$ | 663.1   | 124.6   | -0.5606 |
| $c_{1,i}^{1O}$ | 1728    | -50.97  | 0       |
| $c_{2,i}^{1O}$ | -599    | 32.4    | 0       |
| $c_{0,i}^{3O}$ | 810.6   | -182.7  | -0.7257 |
| $c_{1,i}^{3O}$ | -703.2  | 118.1   | 0       |
| $c_{2,i}^{3O}$ | 209.6   | -13.17  | 0       |

interactions with the ESC08a parametrization is adopted,

$$V_{\Lambda N}^c(k_f; r) = \sum_i^3 (c_{0,i}^c + c_{1,i}^c k_F + c_{2,i}^c k_F^2) \exp\left[-\left(\frac{r}{\beta_i}\right)^2\right], \quad (37)$$

$$V_{\Lambda N}^o(k_f; r) = \sum_i^3 (c_{0,i}^o + c_{1,i}^o k_F + c_{2,i}^o k_F^2) \exp\left[-\left(\frac{r}{\beta_i}\right)^2\right], \quad (38)$$

$$c_{n,i}^c = \frac{1}{4} c_{n,i}^{1E} + \frac{3}{4} c_{n,i}^{3E}, \quad (39)$$

$$c_{n,i}^o = \frac{1}{4} c_{n,i}^{1O} + \frac{3}{4} c_{n,i}^{3O}, \quad (40)$$

with  $\beta_1 = 0.5 \text{ fm}$ ,  $\beta_2 = 0.9 \text{ fm}$ , and  $\beta_3 = 2.0 \text{ fm}$ . Values of the parameters  $c_{n,i}^{1E,3E,1O,3O}$  are listed in Table I. Note that, in the present  $S$ -wave  $\Lambda$  calculation, the effective  $\Lambda$ - $N$  interactions are spin-independent central interactions, as the singlet and triplet parts are averaged with the factors 1/4 and 3/4, respectively, and the spin-orbit interactions are dropped off.

As for the  $k_f$  parameter of the  $\Lambda NG$  interactions, two treatments are adopted. One is the density-dependent interactions with  $k_f = \langle k_f \rangle_\Lambda$ , where  $\langle k_f \rangle_\Lambda$  is the averaged Fermi momentum for the  $\Lambda$  particle,

$$\langle k_f \rangle_\Lambda = \left[ \frac{3\pi^2}{2} \langle \rho_N \rangle_\Lambda \right]^{1/3}, \quad (41)$$

and self-consistently determined for each state. This  $k_f$  choice of the  $\Lambda NG$  interactions is the so-called averaged density approximation (ADA) used in Refs. [40,41,56]. The other is the density-independent interaction with a fixed  $k_f$  value,  $k_f = k_f^{\text{inp}}$ . Here, the input parameter  $k_f^{\text{inp}}$  is chosen for each  $^A_\Lambda Z$  system. It means that the  $k_f^{\text{inp}}$  is system dependent but state independent. In this paper, the mean value of  $\langle k_f \rangle_\Lambda$  of low-energy states obtained by the former treatment (ADA) is used for the input  $k_f^{\text{inp}}$  value. These choices reasonably reproduce the  $\Lambda$  binding energies of  $^7_\Lambda\text{Li}$ ,  $^9_\Lambda\text{Be}$ ,  $^{11}_\Lambda\text{B}$ ,  $^{12}_\Lambda\text{B}$ ,



$^{12}\text{C}$ , and  $^{13}\text{C}$ . The first treatment, density-dependent  $\Lambda NG$  interactions with  $k_f = \langle k_f \rangle_\Lambda$ , is labeled as ESC08a(DD), and the second one, the density-independent  $\Lambda NG$  interactions with  $k_f = k_f^{\text{inp}}$  is labeled as ESC08a(DI). Note that the former is state dependent (structure dependent) and the latter is state independent (structure independent), but the system-dependent  $k_f$  is used in both cases.

The  $\Lambda NG$  interactions have been applied to various structure model calculations of hypernuclei such as cluster model, mean-field, and HAMD calculations. In the application of the  $\Lambda NG$  interactions to cluster model and HAMD calculations, the parameter  $k_f$  of the density-independent  $\Lambda NG$  interactions is usually adjusted to fit the  $\Lambda$  binding energy for each (sub)system. In applications of the effective  $\Lambda NG$  interactions to  $^A_\Lambda Z$  in a wide mass number region, the density-dependent  $\Lambda NG$  interactions have been used, for instance, in the mean-field calculations and recent HAMD calculations [40,41], because they were originally designed in the density-dependent form to reproduce systematics of  $\Lambda$  binding energy [56]. In Refs. [40,56], they also showed the results with another choice of  $k_f = k_f^{\text{LDA2}}$  in addition to the ADA results. In the present calculation for  $(0s)_\Lambda$  states, the results obtained with  $k_f = k_f^{\text{LDA2}}$  show similar results to the present ESC08a(DD) ones.

#### IV. RESULTS

By applying the  $\alpha + d$ ,  $2\alpha$ ,  $2\alpha + d$ ,  $2\alpha + t(h) + p_{3/2}$ , and  $3\alpha + p_{3/2}$  GCM to core nuclei,  $^6\text{Li}$ ,  $^8\text{Be}$ ,  $^{10}\text{B}$ ,  $^{11}\text{B}(\text{C})$ , and  $^{12}\text{C}$ ,  $(0s)_\Lambda$  states in  $^A_\Lambda Z$  is calculated with the single-channel folding potential model by taking account the core polarization effect.

In the present calculation, the  $\Lambda$  particle around the  $I^\pi$  state of the core nucleus  $^{A-1}Z(I^\pi)$  feels the spin-independent potentials, and therefore the spin doublet  $J^\pi = (I \pm 1/2)^\pi$  states in  $^A_\Lambda Z$  completely degenerate. The spin doublet  $J^\pi = (I \pm 1/2)^\pi$  states in  $\Lambda$  hypernuclei are denoted by  $^A_\Lambda Z(I^\pi)$ . Low-lying  $I^\pi$  states with dominant  $0\hbar\omega$  configurations in  $^{A-1}Z$ , and the corresponding  $(0s)_\Lambda$  states in  $^A_\Lambda Z$  are calculated.

The  $^8\text{Be}(0_1^+)$  and  $^6\text{Li}(3_1^+)$  states, which are strictly speaking quasibound states, are calculated in the bound-state approximation with the boundary condition  $d \leq 15$  fm of the GCM model space. The present GCM calculation gives stable results for these states. The  $^8\text{Be}(2_1^+)$  state is a broad resonance state, for which one can not obtain a stable result in the bound-state approximation. Instead, the excitation energy of  $^8\text{Be}(2_1^+)$  is calculated from the  $\alpha + \alpha$  scattering phase shifts with the resonating group method (RGM).

To see the effect of the cluster-breaking component in  $^{A-1}Z$  and  $^A_\Lambda Z$ , I also show some results for  $^{12}\text{C}$  and  $^{13}\text{C}$  obtained by the traditional  $3\alpha$  GCM calculation without the cluster-breaking ( $p_{3/2}$ ) component and compare them with those obtained by the present  $3\alpha + p_{3/2}$  model. Note that, in the present model, the cluster-breaking components contribute only to  $^{12}\text{C}(0^+)$  and  $^{11}\text{B}, \text{C}(3/2^-)$  but do not affect other spin-parity states.

##### A. Properties of core nuclei

Nuclear properties of isolate core nuclei without the  $\Lambda$  particle are shown in Tables II and III. The calculated values of

TABLE II. Energies (MeV), radii (fm), and  $B(E2)$  ( $\text{e}^2\text{fm}^4$ ) in ordinary nuclei. Binding energies ( $-E_N$ ), relative energies ( $E_r$ ) measured from the cluster-decay threshold, calculated rms matter radii ( $R_N$ ), the experimental rms point-proton radii ( $R_p$ ), and  $E2$  transition strengths to the ground states are listed. For  $^{12}\text{C}$ , the results obtained with the present  $3\alpha + p_{3/2}$  model and those with the  $3\alpha$  model without the  $p_{3/2}$  component are shown. The experimental data are from Refs. [65–68].

|                          | $-E_N$ |          | $E_r$  |         | $R_N$ | $R_p$ |
|--------------------------|--------|----------|--------|---------|-------|-------|
|                          | cal    | exp      | cal    | exp     | cal   | exp   |
| $d(1_1^+)$               | 0.43   | 2.224    |        |         | 0.98  | 1.941 |
| $t(1/2_1^+)$             | 6.9    | 8.481    |        |         | 1.23  | 1.504 |
| $\alpha(0_1^+)$          | 27.6   | 28.296   |        |         | 1.55  | 1.410 |
| $^6\text{Li}(1_1^+)$     | 29.5   | 31.995   | − 1.48 | − 1.48  | 2.56  | 2.426 |
| $^8\text{Be}(0_1^+)$     | 55.0   | 56.499   | 0.21   | 0.09    | 3.37  |       |
| $^{10}\text{B}(3_1^+)$   | 60.5   | 64.75    | − 4.88 | − 5.93  | 2.39  | 2.253 |
| $^{11}\text{B}(3/2_1^-)$ | 71.8   | 76.203   | − 9.66 | − 11.13 | 2.33  | 2.229 |
| $^{11}\text{C}(3/2_1^-)$ | 69.2   | 73.439   | − 7.05 | − 8.37  | 2.34  |       |
| $^{12}\text{C}(0_1^+)$   | 90.2   | 92.16    | − 7.37 | − 7.27  | 2.35  | 2.298 |
| w/o $p_{3/2}$            | 88.1   |          | − 3.22 |         | 2.52  |       |
| $B(E2)$                  |        |          |        |         |       |       |
|                          | cal    | exp      |        |         |       |       |
| $^6\text{Li}(3_1^+)$     | 11.3   | 10.7(8)  |        |         |       |       |
| $^{10}\text{B}(1_1^+)$   | 5.2    | 4.15(2)  |        |         |       |       |
| $^{11}\text{B}(5/2_1^-)$ | 9.5    | 8.9(3.2) |        |         |       |       |
| $^{12}\text{C}(2_1^+)$   | 7.3    | 7.6(4)   |        |         |       |       |
| w/o $p_{3/2}$            | 10.6   | 7.6(4)   |        |         |       |       |

the binding energies ( $-E_N$ ), relative energies ( $E_r$ ) measured from cluster break-up threshold energies, root-mean-square (rms) radii of nuclear matter ( $R_N$ ), and  $E2$  transition strengths to the ground states are listed compared with experimental data in Table II. For the experimental data of nuclear radii, the rms radii of point-proton distribution ( $R_p$ ) reduced from the charge radii are shown. I also show the results for  $d$ ,  $t$ , and  $\alpha$  clusters of  $(0s)$  configurations with  $v = 0.235 \text{ fm}^{-2}$ . The energies and sizes are reasonably reproduced by the

TABLE III. The calculated values of rms radii [ $R_N$  (fm)], the size difference [ $R_N - R_{N,\text{gs}}$  (fm)], excitation energies in  $^{11}\text{B}$ , and energy difference from the mirror nucleus  $^{11}\text{C}$ . The difference in the binding energy [ $\Delta_{\text{mir}}(-E_N)$  (MeV)] for the ground state and that in the excitation energies [ $\Delta_{\text{mir}}(E_x)$  (MeV)] for excited states are shown. The experimental data are taken from Ref. [68].

|                          | $R_N$ |                         | $\Delta_{\text{mir}}(\text{B.E})$ |       |                            |      |
|--------------------------|-------|-------------------------|-----------------------------------|-------|----------------------------|------|
|                          |       |                         | cal                               |       | exp                        |      |
| $^{11}\text{B}(3/2_1^-)$ | 2.33  |                         | 2.60                              |       | 2.764                      |      |
|                          | $R_N$ | $R_N - R_{N,\text{gs}}$ | $E_x$                             |       | $\Delta_{\text{mir}}(E_x)$ |      |
|                          |       |                         | cal                               | exp   | cal                        | exp  |
| $^{11}\text{B}(1/2_1^-)$ | 2.50  | 0.18                    | 2.79                              | 2.125 | 0.17                       | 0.13 |
| $^{11}\text{B}(3/2_2^-)$ | 2.58  | 0.26                    | 5.57                              | 5.020 | 0.22                       | 0.22 |
| $^{11}\text{B}(5/2_1^-)$ | 2.51  | 0.19                    | 4.66                              | 4.445 | 0.16                       | 0.13 |

calculation except for the deuteron and triton. The deuteron size is much underestimated, because the fixed-width  $(0s)^2$  configuration is assumed in the present cluster model. The calculated  $B(E2)$  are in agreement with the experimental data without using any effective charges. For  $^{12}\text{C}$ , the  $3\alpha$  GCM calculation without the cluster breaking ( $p_{3/2}$ ) gives a larger size and  $B(E2; 2^+ \rightarrow 0_1^+)$  than those of the present calculation, meaning that  $^{12}\text{C}(0_1^+)$  slightly shrinks because of the cluster-breaking effect as discussed in Ref. [55].

In Table III, I show the Coulomb shift  $\Delta_{\text{mir}}(E_x)$ , which is defined by the excitation energy difference between mirror nuclei, for  $A = 11$  nuclei together with calculated radii. Since the Coulomb interactions give only minor change of nuclear structure, and therefore the Coulomb shift sensitively probes the size difference between the ground and excited states except for weakly bound or resonance states. The calculated Coulomb shifts for  $^{11}\text{B}(1/2_1^-, 3/2_2^-, 5/2_1^-)$  agree well with the experimental data indicating that the size differences of these states are reasonably described by the present calculation.

### B. Ground states of $\Lambda$ hypernuclei

I here discuss the ground-state properties of  $^A_\Lambda Z$ . In  $^A_\Lambda Z$ , the nuclear size  $R_N$  ( $R_N$  is the rms nuclear matter radius measured from the cm of the core nucleus) slightly decreases and the nuclear energy  $E_N$  slightly increases from the original size ( $R_N^{\text{up}}$ ) and energy ( $E_N^{\text{up}}$ ) of unperturbative core nuclei  $^{A-1}Z$  without the  $\Lambda$ . I calculate the nuclear size change  $\delta_\Lambda(R_N) = R_N - R_N^{\text{up}}$  and the nuclear energy change  $\delta_\Lambda(E_N) = E_N - E_N^{\text{up}}$  caused by the  $\Lambda$  particle in  $^A_\Lambda Z$ . To see the core polarization effect, I also calculate the  $\Lambda$  energy gain,  $\Delta_{\text{cp}}(E_\Lambda) = E_\Lambda(\epsilon) - E_\Lambda(\epsilon = 0)$ , defined by the energy difference between the calculations with and without the core polarization. Here  $E_\Lambda(\epsilon = 0)$  is the  $\Lambda$  energy without the core polarization, that is the  $\Lambda$  energy in the  $\Lambda$ -( $^{A-1}Z$ ) system with the unperturbative core nucleus.

In Table IV, I show the calculated results of the ground-state properties of  $^A_\Lambda Z$  together with the experimental  $B_\Lambda$ . As reference data, I also show the results for  $^5_\Lambda\text{He}$  obtained by the  $\Lambda$ - $\alpha$  calculation with the inert  $\alpha$  core assumption. Systematics of  $\Lambda$  binding energies in this mass-number region is reasonably reproduced in both ESC08a(DI) and ESC08a(DD) interactions, though the reproduction is not perfect.

For  $A > 10$  systems, the nuclear size change  $\delta_\Lambda(R_N)$  is less than 5%. The small size change of the core nucleus in the ground state of  $^{13}_\Lambda\text{C}$  is consistent with the prediction of other calculations [4,5,9,13,20]. Moreover, the nuclear energy change  $\delta_\Lambda(E_N)$  and  $\Lambda$  energy gain  $\Delta_{\text{cp}}(E_\Lambda)$  by the core polarization are also small and compensate each other. It indicates that the core polarization effect is minor and regarded as a higher-order perturbation in the  $\Lambda$  binding except for  $A < 10$  systems. The core polarization effects in the ESC08a(DD) results for  $A > 10$  systems are particularly small, because the ESC08a(DD) interactions become weak as the nuclear density increases because of the  $k_f$  dependence.

As explained previously, the core polarization effect is taken into account by changing the enhancement factor  $\epsilon$ , which can be regarded as a control parameter of the nuclear size  $R_N$ . In Fig. 1, I show the nuclear size dependence of

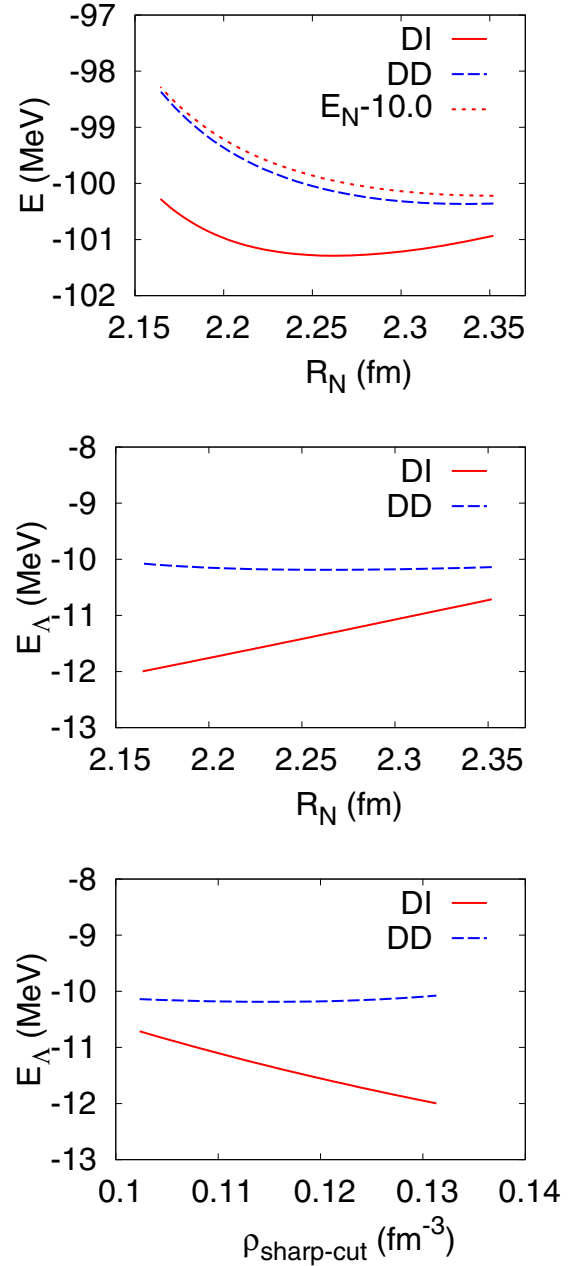


FIG. 1. Total energy [ $E(\epsilon) = E_N(\epsilon) + E_\Lambda(\epsilon)$ ] and  $\Lambda$  energy [ $E_\Lambda(\epsilon)$ ] for polarized core  $\Phi(\epsilon)$  in  $^{13}_\Lambda\text{C}(0_1^+)$ . The energies are plotted against the rms nuclear matter radius  $R_N(\epsilon)$  in the top and middle panels. The nuclear energy [ $E_N(\epsilon)$ ] subtracted by 10 MeV is also shown.  $E_\Lambda(\epsilon)$  plotted to the sharp-cut density  $\rho_{\text{sharp-cut}} = (3/4\pi)(3/5)^{3/2}AR_N^{-3}$  reduced from  $R_N(\epsilon)$  for the uniform density ansatz is shown in the bottom panel. The calculated values obtained with ESC08a(DI) and ESC08a(DD) are shown.

$E_N(\epsilon)$ ,  $E_\Lambda(\epsilon)$ , and  $E(\epsilon) = E_N(\epsilon) + E_\Lambda(\epsilon)$  in  $^{13}_\Lambda\text{C}$  obtained by varying the enhancement factor  $\epsilon$ . The energies are plotted as functions of the nuclear size  $R_N(\epsilon)$ . The  $R_N^{-3}$  dependence of  $E_\Lambda(\epsilon)$  is also shown. In the ESC08a(DI) result, the  $\Lambda$  energy ( $E_\Lambda$ ) gradually goes down with the nuclear size reduction because the higher nuclear density gives larger attraction to the  $\Lambda$  potentials. As a result, the  $\Lambda$  particle slightly reduces

TABLE IV. Ground-state properties of  $\Lambda$  hypernuclei. The  $\Lambda$  distribution size [ $r_\Lambda$  (fm)], averaged Fermi momentum ( $\langle k_f \rangle_\Lambda$  fm $^{-1}$ ), core nuclear size [ $R_N$  (fm)], nuclear size change [ $\delta_\Lambda(R_N)$  (fm)], nuclear energy change [ $\delta_\Lambda(E_N)$  (MeV)], difference of  $\Lambda$  energy with and without core polarization [ $\Delta_{cp}(E_\Lambda)$  (MeV)], and the  $\Lambda$  binding energy [ $B_\Lambda$  (MeV)] are listed. The calculated results obtained with ESC08a(DI) and ESC08a(DD) are shown. The experimental  $B_\Lambda$  values are taken from the data compilation in Ref. [70]. The experimental data of spin-averaged values [ $\overline{B}_\Lambda$  (MeV)] of the  $\Lambda$  binding energy for spin doublets,  $J^\pi = I^\pi \pm 1/2$ , are also shown. The experimental data of the spin doublet splitting are taken from Refs. [2,48,74,77].

| ESC08a(DI)                     |                    |             |                               |       |                       |                       |                          |             |                          |                                     |
|--------------------------------|--------------------|-------------|-------------------------------|-------|-----------------------|-----------------------|--------------------------|-------------|--------------------------|-------------------------------------|
|                                | $k_f^{\text{inp}}$ | $r_\Lambda$ | $\langle k_f \rangle_\Lambda$ | $R_N$ | $\delta_\Lambda(R_N)$ | $\delta_\Lambda(E_N)$ | $\Delta_{cp}(E_\Lambda)$ | $B_\Lambda$ | $B_{\Lambda,\text{exp}}$ | $\overline{B}_{\Lambda,\text{exp}}$ |
| $^5_\Lambda\text{He}(0^+)$     | 0.95               | 2.84        | 0.95                          | 1.55  |                       |                       |                          | 3.6         | 3.12(2)                  | 3.12(2)                             |
| $^7_\Lambda\text{Li}(1^+)$     | 0.93               | 2.57        | 0.95                          | 2.22  | -0.33                 | 0.59                  | -0.85                    | 5.4         | 5.58(3)                  | 5.12(3)                             |
| $^9_\Lambda\text{Be}(0^+)$     | 0.90               | 2.44        | 0.98                          | 2.44  | -0.94                 | 1.69                  | -3.15                    | 7.0         | 6.71(4)                  | 6.71(4)                             |
| $^{11}_\Lambda\text{B}(3^+)$   | 1.03               | 2.36        | 1.10                          | 2.29  | -0.10                 | 0.37                  | -0.42                    | 10.0        | 10.24(5)                 | 10.09(5)                            |
| $^{12}_\Lambda\text{B}(3/2^-)$ | 1.07               | 2.33        | 1.16                          | 2.24  | -0.09                 | 0.29                  | -0.36                    | 10.9        | 11.37(6)                 | 11.27(6)                            |
| $^{12}_\Lambda\text{C}(3/2^-)$ | 1.06               | 2.32        | 1.16                          | 2.25  | -0.09                 | 0.31                  | -0.42                    | 11.1        | 10.76(19)                | 10.65(19)                           |
| $^{13}_\Lambda\text{C}(0^+)$   | 1.11               | 2.35        | 1.18                          | 2.26  | -0.09                 | 0.27                  | -0.36                    | 11.1        | 11.69(12)                | 11.69(12)                           |
| w/o $p_{3/2}$                  | 1.11               | 2.45        | 1.11                          | 2.41  | -0.11                 | 0.35                  | -0.42                    | 9.9         | 11.69(12)                | 11.69(12)                           |
| ESC08a(DD)                     |                    |             |                               |       |                       |                       |                          |             |                          |                                     |
|                                |                    | $r_\Lambda$ | $\langle k_f \rangle_\Lambda$ | $R_N$ | $\delta_\Lambda(R_N)$ | $\delta_\Lambda(E_N)$ | $\Delta_{cp}(E_\Lambda)$ | $B_\Lambda$ | $B_{\Lambda,\text{exp}}$ | $\overline{B}_{\Lambda,\text{exp}}$ |
| $^5_\Lambda\text{He}(0^+)$     |                    | 2.83        | 0.95                          | 1.55  |                       |                       |                          | 3.6         | 3.12(2)                  | 3.12(2)                             |
| $^7_\Lambda\text{Li}(1^+)$     |                    | 2.66        | 0.91                          | 2.40  | -0.15                 | 0.08                  | -0.12                    | 5.4         | 5.58(3)                  | 5.12(3)                             |
| $^9_\Lambda\text{Be}(0^+)$     |                    | 2.67        | 0.90                          | 2.69  | -0.68                 | 0.44                  | -1.19                    | 6.4         | 6.71(4)                  | 6.71(4)                             |
| $^{11}_\Lambda\text{B}(3^+)$   |                    | 2.48        | 1.06                          | 2.38  | -0.01                 | 0.00                  | 0.00                     | 9.0         | 10.24(5)                 | 10.09(5)                            |
| $^{12}_\Lambda\text{B}(3/2^-)$ |                    | 2.45        | 1.11                          | 2.33  | 0.00                  | 0.00                  | 0.00                     | 9.6         | 11.37(6)                 | 11.27(6)                            |
| $^{12}_\Lambda\text{C}(3/2^-)$ |                    | 2.45        | 1.11                          | 2.34  | 0.00                  | 0.00                  | 0.00                     | 9.6         | 10.76(19)                | 10.65(19)                           |
| $^{13}_\Lambda\text{C}(0^+)$   |                    | 2.44        | 1.13                          | 2.35  | 0.00                  | 0.00                  | 0.00                     | 10.1        | 11.69(12)                | 11.69(12)                           |
| w/o $p_{3/2}$                  |                    | 2.47        | 1.08                          | 2.51  | -0.01                 | 0.01                  | -0.01                    | 10.1        | 11.69(12)                | 11.69(12)                           |

the core nuclear size. In contrast, in the ESC08a(DD) result, the  $\Lambda$  energy has almost no dependence on the nuclear size, because the density dependence of the  $\Lambda NG$  interactions compensates the  $\Lambda$  energy gain in the higher nuclear density. As a result, the  $\Lambda$  particle hardly changes the core nucleus size. Namely, the density dependence of the ESC08a(DD) interactions suppresses the size reduction of the core nuclei.

Let me turn to  $A < 10$  systems,  $^7_\Lambda\text{Li}$  and  $^9_\Lambda\text{Be}$ . Differently from  $A > 10$  systems, rather significant core size reduction occurs, because  $^6\text{Li}$  and  $^8\text{Be}$  have spatially developed  $\alpha + d$ - and  $2\alpha$ -cluster structures, respectively, and they are rather fragile (soft) against the size reduction. This is consistent with the size shrinkage predicted by pioneering works in Refs. [4,5] followed by many works (see a review paper [13] and references therein). Particularly remarkable core polarization effects are found in  $^9_\Lambda\text{Be}$ , because  $^8\text{Be}$  is a very fragile system of the loosely bound (strictly speaking, quasibound)  $2\alpha$  state. The core polarization effects are seen in the nuclear size change  $\delta_\Lambda(R_N)$  and also the energy changes,  $\delta_\Lambda(E_N)$  and  $\delta_\Lambda(E_\Lambda)$ , in both ESC08a(DI) and ESC08a(DD) calculations. For  $^7_\Lambda\text{Li}$ , the core size reduction is 13% in the ESC08a(DI) result, whereas it is 6% in the ESC08a(DD) result. It should be commented that the size reduction discussed here is the reduction of nuclear matter radii of core nuclei. Detailed discussions of the shrinkage of the intercluster distance in  $^7_\Lambda\text{Li}$  and  $^9_\Lambda\text{Be}$  are given later.

It is worth discussing the size reduction effect on the energy balance between the nuclear energy increase and the  $\Lambda$  energy gain in a perturbative evaluation. In the small size reduction limit, the simple relation

$$\Delta_{cp}(E_\Lambda) = -2\delta_\Lambda(E_N) \quad (42)$$

is easily obtained from the energy balance as explained in Ref. [69]. The relation should be fulfilled if the size reduction is small enough. However, the calculated values of  $\Delta_{cp}(E_\Lambda)$  and  $\delta_\Lambda(E_N)$  in the ESC08a(DI) result somewhat deviate from the relation even in  $A \leq 10$  nuclei because  $\geq 4\%$  size reduction is not enough small as to be treated as the ideal perturbation.

### C. Excited states of $\Lambda$ hypernuclei

I also apply the present method to core-excited  $(0s)_\Lambda$  states in  $\Lambda$  hypernuclei. A particular attention is paid to excitation energy shift and its relation to nuclear size difference from the ground state in each  $^A_Z$  system.

#### 1. Sizes and $E2$ strengths

In Table V, the calculated values of the  $\Lambda$  distribution size  $r_\Lambda$ , averaged Fermi momentum  $\langle k_f \rangle_\Lambda$ , core nuclear size  $R_N$ , and nuclear size change  $\delta_\Lambda(R_N)$  for excited states obtained with ESC08a(DI) are shown. The nuclear size change  $\delta_\Lambda(R_N)$  for excited states shows similar trend to that for the ground

TABLE V. Properties of excited states in  $\Lambda$  hypernuclei. The  $\Lambda$  distribution size [ $r_\Lambda$  (fm)], averaged Fermi momentum [ $\langle k_f \rangle_\Lambda$  (fm $^{-1}$ )], core nuclear size [ $R_N$  (fm)], nuclear size change [ $\delta_\Lambda(R_N)$  (fm)], the difference  $R_N - R_{N,\text{gs}}$  (fm) of the nuclear size from that of the ground state, excitation energies in  $A^{-1}Z$  and  ${}^\Lambda_Z$  systems [ ${}^{A-1}E_x$  and  ${}^\Lambda E_x$  (MeV)], and the excitation energy shift  $\delta_\Lambda(E_x)$  (MeV). The calculated values obtained with ESC08a(DI) are shown together with  $\delta_\Lambda(E_x)$  calculated with ESC08a(DD). For details of the experimental data of excitation energies, see the caption of Fig. 2.

|                                  | $r_\Lambda$ | $\langle k_f \rangle_\Lambda$ | $R_N$ | $\delta_\Lambda(R_N)$ | $R_N - R_{N,\text{gs}}$ | ${}^{A-1}E_x$       | ${}^{A-1}E_{x,\text{exp}}$ | ${}^\Lambda E_x$ | ${}^\Lambda E_{x,\text{exp}}$ | $\delta_\Lambda(E_x)$ | $\delta_\Lambda(E_x)_{\text{DD}}$ | $\delta_\Lambda(E_x)_{\text{exp}}$ |
|----------------------------------|-------------|-------------------------------|-------|-----------------------|-------------------------|---------------------|----------------------------|------------------|-------------------------------|-----------------------|-----------------------------------|------------------------------------|
| ${}^7_\Lambda\text{Li}(3^+)$     | 2.42        | 1.02                          | 2.04  | -0.41                 | -0.19                   | 2.08                | 2.19                       | 0.89             | 1.86                          | -1.19                 | -0.21                             | -0.33                              |
| ${}^9_\Lambda\text{Be}(2^+)$     | 2.41        | 0.99                          | 2.42  | -3.39                 | -0.02                   | 3.11 <sup>RGM</sup> | 3.04                       | 2.68             | 3.04                          | -0.43 <sup>RGM</sup>  | -0.29 <sup>RGM</sup>              | 0                                  |
| ${}^{11}_\Lambda\text{B}(1^+)$   | 2.50        | 1.03                          | 2.47  | -0.12                 | 0.18                    | 1.21                | 0.72                       | 2.72             | 1.67                          | 1.51                  | 0.23                              | 0.95                               |
| ${}^{12}_\Lambda\text{B}(1/2^-)$ | 2.44        | 1.09                          | 2.40  | -0.10                 | 0.16                    | 2.79                | 2.13                       | 4.13             | 3.00                          | 1.34                  | 0.02                              | 0.87 (1 $^-$ )                     |
| ${}^{12}_\Lambda\text{B}(3/2^-)$ | 2.48        | 1.06                          | 2.46  | -0.12                 | 0.22                    | 5.57                | 5.02                       | 7.45             | 6.02                          | 1.88                  | 0.11                              | 1.00*                              |
| ${}^{12}_\Lambda\text{B}(5/2^-)$ | 2.44        | 1.09                          | 2.40  | -0.11                 | 0.16                    | 4.66                | 4.45                       | 6.05             |                               | 1.39                  | 0.03                              |                                    |
| ${}^{12}_\Lambda\text{C}(1/2^-)$ | 2.43        | 1.09                          | 2.41  | -0.11                 | 0.16                    | 2.62                | 2.00                       | 4.01             | 2.73                          | 1.39                  | 0.04                              | 0.73 (1 $^-$ )                     |
| ${}^{12}_\Lambda\text{C}(3/2^-)$ | 2.48        | 1.06                          | 2.48  | -0.12                 | 0.23                    | 5.35                | 4.80                       | 7.30             | 5.81                          | 1.96                  | 0.13                              | 1.01*                              |
| ${}^{12}_\Lambda\text{C}(5/2^-)$ | 2.43        | 1.09                          | 2.41  | -0.11                 | 0.16                    | 4.50                | 4.32                       | 5.94             |                               | 1.44                  | 0.05                              |                                    |
| ${}^{13}_\Lambda\text{C}(2^+)$   | 2.44        | 1.12                          | 2.39  | -0.10                 | 0.13                    | 4.47                | 4.44                       | 5.50             | 4.89                          | 1.03                  | -0.04                             | 0.45 (3/2 $^+$ )                   |
| w/o $p_{3/2}$                    | 2.44        | 1.12                          | 2.39  | -0.10                 | -0.02                   | 2.36                | 4.44                       | 2.19             | 4.89                          | -0.17                 | -0.01                             | 0.45 (3/2 $^+$ )                   |

states. Namely, slight reduction of the nuclear size occurs in  ${}^A_\Lambda Z$  for  $A > 10$ . In  ${}^7_\Lambda\text{Li}$ , significant size reduction occurs also in the excited state,  ${}^7_\Lambda\text{Li}(3^+)$ , because of the spatially developed  $\alpha + d$  clustering.  ${}^8_\Lambda\text{Be}(2^+)$  is a broad resonance, but it is bound in  ${}^9_\Lambda\text{Be}(2^+)$  because of the  $\Lambda$  attraction.

Table VI shows the  $E2$  transition strengths calculated with ESC08a(DI). The  $B(E2; I_i^\pm \rightarrow I_f^\pm, \text{core})$  of the core nuclear part in  ${}^A_\Lambda Z$  are shown compared with the original  $B(E2)$  in  ${}^{A-1}Z$  systems without the  $\Lambda$  particle.  $B(E2, \text{core})$  in  ${}^A_\Lambda Z$  is generally smaller than the original  $B(E2)$  in  ${}^{A-1}Z$  because of the nuclear size reduction. I also show the size reduction factor  $S_{E2}$  reduced from the ratio of  $B(E2; I_i^\pm \rightarrow I_f^\pm, \text{core})$  in  ${}^A_\Lambda Z$  to the unperturbative value,  $B(E2; I_i^\pm \rightarrow I_f^\pm)$  in  ${}^{A-1}Z$ , as  $S_{E2} = [B(E2; I_i^\pm \rightarrow I_f^\pm, \text{core})/B(E2; I_i^\pm \rightarrow I_f^\pm)]^{1/4}$ . In  $A > 10$  systems, the  $B(E2)$  reduction is not as remarkable as that in  $A < 10$  systems because of the small size reduction in the

ground and excited states. By contrast,  $B(E2)$  is remarkably reduced in  ${}^7_\Lambda\text{Li}$  as a result of the significant size reduction in the ground and excited states. This is nothing but the famous phenomenon of the so-called gluelike role of the  $\Lambda$  particle [4,5]. The calculated  $B(E2; 3^+ \rightarrow 1^+, \text{core})$  in  ${}^7_\Lambda\text{Li}$  and  $B(E2; 3^+ \rightarrow 1^+)$  in  ${}^6\text{Li}$  agree with the experimental data. Detailed discussions are given later.

## 2. Excitation energy and size difference

In Table VI, excitation energies ( $E_x$ ) in  ${}^{A-1}Z$  and  ${}^A_\Lambda Z$  are listed. The calculated and experimental energy spectra are shown in Fig. 2. To see the effects of the  $\Lambda$  particle on excitation energies, I also show the excitation energy shift  $\delta_\Lambda(E_x) = E_x[{}^A_\Lambda Z(I^\pi)] - E_x[{}^{A-1}Z(I^\pi)]$  in Table VI.

The ESC08a(DI) result shows the significant energy shift and qualitatively describes the systematic trend of the experimental energy shift. The energy shift comes from the size difference between the ground and excited states because a  $\Lambda$  particle experiences a deeper potential in a higher nuclear density system through the  $\Lambda$ - $N$  interactions. As shown in Table V, the excitation energy shift  $\delta_\Lambda(E_x)$  clearly correlates with the size difference  $R_N - R_{N,\text{gs}}$ , where  $R_{N,\text{gs}}$  is the size of the ground state. Namely, the excitation energies shift upward reflecting the larger sizes of excited states in  $A > 10$  systems. Note that, in  $A > 10$  systems, the size difference in  ${}^A_\Lambda Z$  is consistent with that in  ${}^{A-1}Z$  meaning that the origin of the size difference, i.e., the excitation energy shift, is the structure difference between the ground and excited states in original core nuclei  ${}^{A-1}Z$ . The excited state  ${}^{10}\text{B}(1^+)$  has a developed  $2\alpha + d$  cluster, and has a larger size than that of the ground state  ${}^{10}\text{B}(3^+)$  with a weaker clustering because of the stronger spin-orbit attraction of the  $d$  cluster as discussed in Refs. [79,80]. The excited states of  ${}^{11}\text{B}$  and  ${}^{11}\text{C}$  have the  $2\alpha + t$  and  $2\alpha + {}^3\text{He}$  cluster structures, and have larger sizes than those of the ground states  ${}^{11}\text{B}(3/2^+)$  and  ${}^{11}\text{C}(3/2^+)$ , respectively, which are reduced by the cluster breaking ( $p_{3/2}$ )

TABLE VI.  $B(E2)$  (e $^2\text{fm}^4$ ) for  $I_i^\pi \rightarrow \text{g.s.}$  in  ${}^{A-1}Z$  and  ${}^A_\Lambda Z$ . For  ${}^A_\Lambda Z$ , the  $E2$  transition strengths in the core nuclear part  $B(E2, \text{core})$  are shown. The reduction factor  $S_{E2}$  is also shown. The experimental  $B(E2; \text{core})$  for  ${}^7_\Lambda\text{Li}$  is evaluated from the experimental  $B(E2; 5/2^+ \rightarrow 1/2^+)$  [48] by scaling the spin factor 9/7 as  $B(E2; 3^+ \rightarrow 1^+, \text{core}) = (9/7)B(E2; 5/2^+ \rightarrow 1/2^+)$ . The experimental data for  ${}^{A-1}Z$  nuclei are from Refs. [65–68].

| ${}^{A-1}Z(I_i^\pi)$     | $B(E2)$ |          | ${}^A_\Lambda Z(I_i^\pi)$        | $B(E2, \text{core})$ |          | $S_{E2}$ |         |
|--------------------------|---------|----------|----------------------------------|----------------------|----------|----------|---------|
|                          | cal     | exp      |                                  | cal                  | exp      | cal      | exp     |
| ${}^6\text{Li}(3^+)$     | 11.3    | 10.7(8)  | ${}^7_\Lambda\text{Li}(3^+)$     | 3.4                  | 4.6(1.3) | 0.74     | 0.81(4) |
| ${}^8\text{Be}(2^+)$     |         |          | ${}^9_\Lambda\text{Be}(2^+)$     | 15.2                 |          |          |         |
| ${}^{10}\text{B}(1^+)$   | 5.2     | 4.15(2)  | ${}^{11}_\Lambda\text{B}(1^+)$   | 3.1                  |          | 0.88     |         |
| ${}^{11}\text{B}(5/2^-)$ | 9.5     | 8.9(3.2) | ${}^{12}_\Lambda\text{B}(5/2^-)$ | 4.5                  |          | 0.83     |         |
| ${}^{12}\text{C}(2^+)$   | 7.3     | 7.6(4)   | ${}^{13}_\Lambda\text{C}(2^+)$   | 5.0                  |          | 0.91     |         |
| w/o $p_{3/2}$            | 10.6    |          |                                  | 7.8                  |          | 0.93     |         |



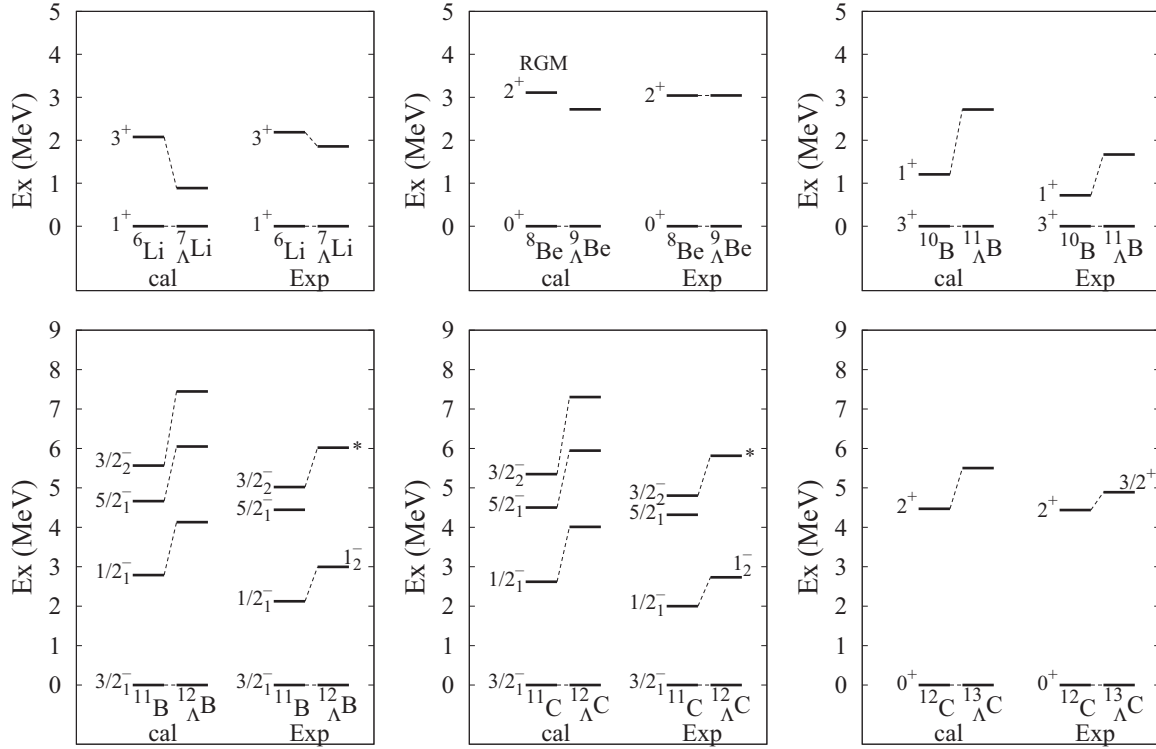


FIG. 2. Energy spectra calculated with ESC08a(DI) and the experimental spectra. The experimental data for  $A^{-1}Z$  are from Refs. [65–68], and those for  $A Z$  are taken from Refs. [2,48,71–78]. The excitation energy of  ${}^8\text{Be}(2^+)$  is calculated by the RGM calculation. The experimental data for  $A Z$  are the spin-averaged values reduced from the excitation energies of spin doublets,  $J^\pi = I^\pi \pm 1/2$ , except for  ${}^{12}\text{B}(1/2_1^-, 3/2_2^-)$ ,  ${}^{12}\text{C}(1/2_1^-, 3/2_2^-)$ , and  ${}^{12}\text{C}(2^+)$ . For  ${}^{12}\text{B}(1/2_1^-)$ ,  ${}^{12}\text{C}(1/2_1^-)$ , and  ${}^{12}\text{C}(2^+)$ , the experimental values of  $E_x(1^-)$ ,  $E_x(1^-)$ , and  $E_x(3/2^+)$  are used, respectively. For  ${}^{12}\text{B}(3/2_2^-)$ , the experimental values of  $E_x(1^-)$  in  ${}^{12}\text{B}$  and  $E_x(2^-)$  in  ${}^{12}\text{C}$  are averaged by assuming that the Coulomb shift in  ${}^{12}\text{B}(3/2_2^-)$ – ${}^{12}\text{C}(3/2_2^-)$  is the same value as that in  ${}^{11}\text{B}(3/2_2^-)$ – ${}^{11}\text{C}(3/2_2^-)$ .

component. Also in  ${}^{12}\text{C}$ , the excited state  ${}^{12}\text{C}(2_1^+)$  has the  $3\alpha$  cluster structure and the larger size than that of the ground state, in which significant mixing of the cluster-breaking component reduces the size of the ground state. In  ${}^7\text{Li}$ , the situation is opposite. The excited states,  ${}^6\text{Li}(3_1^+)$  and  ${}^7\text{Li}(3_1^+)$  have smaller sizes than those of the ground states,  ${}^6\text{Li}(1_1^+)$  and  ${}^7\text{Li}(1_1^+)$ , because of the higher centrifugal barrier in addition to the stronger spin-orbit attraction between  $\alpha$  and  $d$  clusters in the  $D$ -wave  $\alpha + d$  state than in the  $S$ -wave state. Reflecting the smaller size than the ground state, the excitation energy of  ${}^7\text{Li}(3_1^+)$  shifts downward. For  ${}^9\text{Be}$ , it is difficult to give a quantitative discussion of the energy shift because  ${}^8\text{Be}(2^+)$  is the broad resonance.

For  ${}^{13}\text{C}$ , the traditional  $3\alpha$  calculation without the cluster breaking gives a result different from the present result obtained by the  $3\alpha + p_{3/2}$  calculation. In the traditional  $3\alpha$  calculation, the ground state has the  $3\alpha$  cluster structure with no cluster breaking and almost the same or even slightly larger size than the excited state. The comparable sizes between the ground and excited states are reflected in the small excitation energy shift in  ${}^{13}\text{C}(2_1^+)$  in the traditional  $3\alpha$  calculation. This contradicts to the present result and is inconsistent with the experimental data. It should be commented that traditional  $3\alpha$ -cluster models generally obtain a slightly smaller size of  ${}^{12}\text{C}(2_1^+)$  than the ground state. For example, the size of  ${}^{12}\text{C}(2_1^+)$  and that of  ${}^{12}\text{C}(0_1^+)$  are 2.38 fm and 2.40 fm in

the  $3\alpha$  RGM calculation [81] (2.50 fm and 2.53 fm in the  $3\alpha$  GCM calculation [63,64]). It means that cluster-breaking components in core nuclei can affect the excitation energy shift in  $A Z$  systems.

In order to look into the dependence of the excitation energy shift on the size difference in more detail, the energy shift and the size difference are plotted in Fig. 3. The ESC08a(DI) results show a clear correlation between the energy shift and the size difference. Namely, the larger size, the larger energy shift. The calculation qualitatively describes the systematic trend of the experimental data. However, quantitatively, it overestimates the experimental energy shift by a factor of 1.5–2.

Although it is generally difficult to experimentally measure sizes of excited states in  $A^{-1}Z$  systems, one can obtain information from the Coulomb shift in mirror nuclei. As described previously, the present calculation reasonably reproduces the experimental Coulomb shift in  ${}^{11}\text{B}$ – ${}^{11}\text{C}$ . Roughly speaking, about 0.2 fm size difference describes  $\sim 0.2$  MeV Coulomb shift in  ${}^{11}\text{B}$ – ${}^{11}\text{C}$ , whereas it gives  $\sim 1$  MeV energy shift in  ${}^{12}\text{B}$  ( ${}^{12}\text{C}$ ). Namely, the size difference causes about five times larger energy difference in the  $\Lambda$  energy than that in the Coulomb energy.

The energy shift and size difference calculated without the core polarization are also shown in Fig. 3 by open circles. They are almost consistent with the results with the core polarization because the core polarization (size reduction) effect on energy

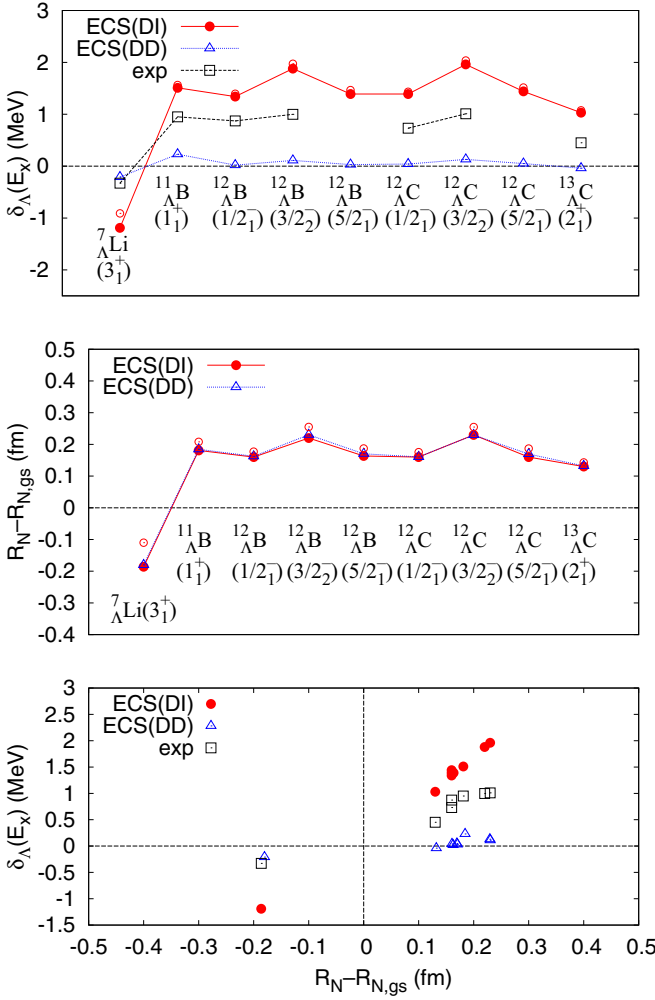


FIG. 3. (Top) Excitation energy shift  $\delta_\Lambda(E_x)$  calculated with ESC08a(DI) and ESC08a(DD), and experimental values. The excitation energy shift without the core polarization calculated with ESC08a(DI) is also plotted by open circles. (Middle) Nuclear size difference ( $R_N - R_{N,gs}$ ) of excited states from that of the ground states obtained with ESC08a(DI) and ESC08a(DD). The result without the core polarization calculated with ESC08a(DI) is also shown by open circles. (Bottom) The excitation energy shift plotted against the nuclear size difference obtained with ESC08a(DI) and ESC08a(DD). Experimental energy shift is plotted against the theoretical size difference calculated with ESC08a(DI).

is higher-order perturbation. In other words, the origin of the excitation energy shift in  ${}^A_\Lambda Z$  is, in the leading order, the nuclear size difference between the ground and excited states in the original (unperturbative) core nuclei  ${}^{A-1}Z$ . It turns out that the excitation energy shift in  $\Lambda$  hypernuclei can probe the size difference between the ground and excited states in original  ${}^{A-1}Z$  nuclei in this mass-number region.

In contrast to the significant energy shift in the ESC08a(DI) results, the ESC08a(DD) results show almost no energy shift and fails to describe the systematic trend of the experimental energy shift as shown in Table V and Fig. 3. In the case of ESC08a(DD), the  $\Lambda$  energy in  ${}^A_\Lambda Z$  has no (or

only weak) dependence on the nuclear size because of the density ( $k_f$ ) dependence of the  $\Lambda NG$  interactions as discussed previously, and therefore, the  $\Lambda$  particle can not probe the nuclear size difference between the ground and excited states.

As seen in the bottom panel of Fig. 3, the systematic trend of the experimental energy shift can be described by the ESC08a(DI) calculation but not by the ESC08a(DD) calculation, meaning that the density-independent  $\Lambda NG$  interactions are rather favored than the density-dependent ones. However, as for the quantitative reproduction, the ESC08a(DI) calculation generally overestimates the experimental energy shift by a factor of 1.5–2. It is likely that weak density dependence of the  $\Lambda NG$  interactions may be suitable for detailed description of the excitation energy shift in  ${}^A_\Lambda Z$ .

Earlier works with semimicroscopic  $\alpha + d + \Lambda$  cluster models in Ref. [4,11] give the spin-averaged excitation energy shift  $\delta_\Lambda(E_x) = -0.34$  MeV [4] and  $-0.46$  MeV [11] for  ${}^7_\Lambda\text{Li}(3_1^+)$ . The negative values of the excitation energy shift and a smaller size than the ground state  ${}^7_\Lambda\text{Li}(1_1^+)$  are consistent with the present result. For  ${}^9_\Lambda\text{Be}(2_1^+)$ , the semimicroscopic  $2\alpha + \Lambda$  cluster model calculations give  $\delta_\Lambda(E_x) = 0$  MeV [4] and  $-0.08$  MeV [11]. The theoretical results describe well the experimental values of the excitation energy shift.

## V. DISCUSSIONS

### A. Density distributions

Figure 4 shows the distribution functions of the  $\Lambda$  density  $\rho_\Lambda(r)$  and nuclear density  $\rho_N(r)$  in the ground and excited states of  ${}^A_\Lambda Z$  as functions of  $r$ . Note that  $r$  is the distance from the cm of core nuclei. The figures also show the  $\Lambda$  density  $\rho_\Lambda^{\text{up}}(r)$  and nuclear density  $\rho_N^{\text{up}}(r)$  in  $\Lambda$ -( ${}^{A-1}Z$ ) systems with unperturbative core nuclei (without core polarization).  $\rho_N^{\text{up}}(r)$  is the original nuclear density in isolated  ${}^{A-1}Z$  systems without the  $\Lambda$  particle.

Let me discuss the  $\Lambda$  density shown in the left panels of Fig. 4. As seen in the small difference between  $\rho_\Lambda(r)$  and  $\rho_\Lambda^{\text{up}}(r)$ , the core polarization effect on the  $\Lambda$  distribution is rather minor except for  ${}^9_\Lambda\text{Be}$ . Moreover, the difference between the ground and excited states in each system is also small. The center  $\Lambda$  density increases as the mass number  $A$  increases reflecting the deeper  $\Lambda$  binding in heavier systems.

Let me look at the nuclear density shown in the middle and right panels of Fig. 4. Compared with the original density  $\rho_N^{\text{up}}(r)$  in  ${}^{A-1}Z$  systems, the nuclear density  $\rho_N(r)$  in  ${}^A_\Lambda Z$  is slightly increased in  $A > 10$  systems, and rather significantly enhanced in  $A < 10$  systems, as the result of the size reduction discussed previously.

In comparison with the nuclear density between the ground and excited states in each system, one finds significant difference between them except for  ${}^9_\Lambda\text{Be}$ . In  $A > 10$  systems, the inner density (typically in the  $r \lesssim 2$  fm region) is lower in excited states than in the ground states. The situation is opposite in  ${}^7_\Lambda\text{Li}$ . The  ${}^7_\Lambda\text{Li}(3_1^+)$  has the higher inner density than that of  ${}^7_\Lambda\text{Li}(1_1^+)$ . As shown by green lines in right panels of Fig. 4, the  $r^2$ -weighted  $\rho_\Lambda(r)$  has a maximum peak at  $r = 1.5 \sim 2.0$

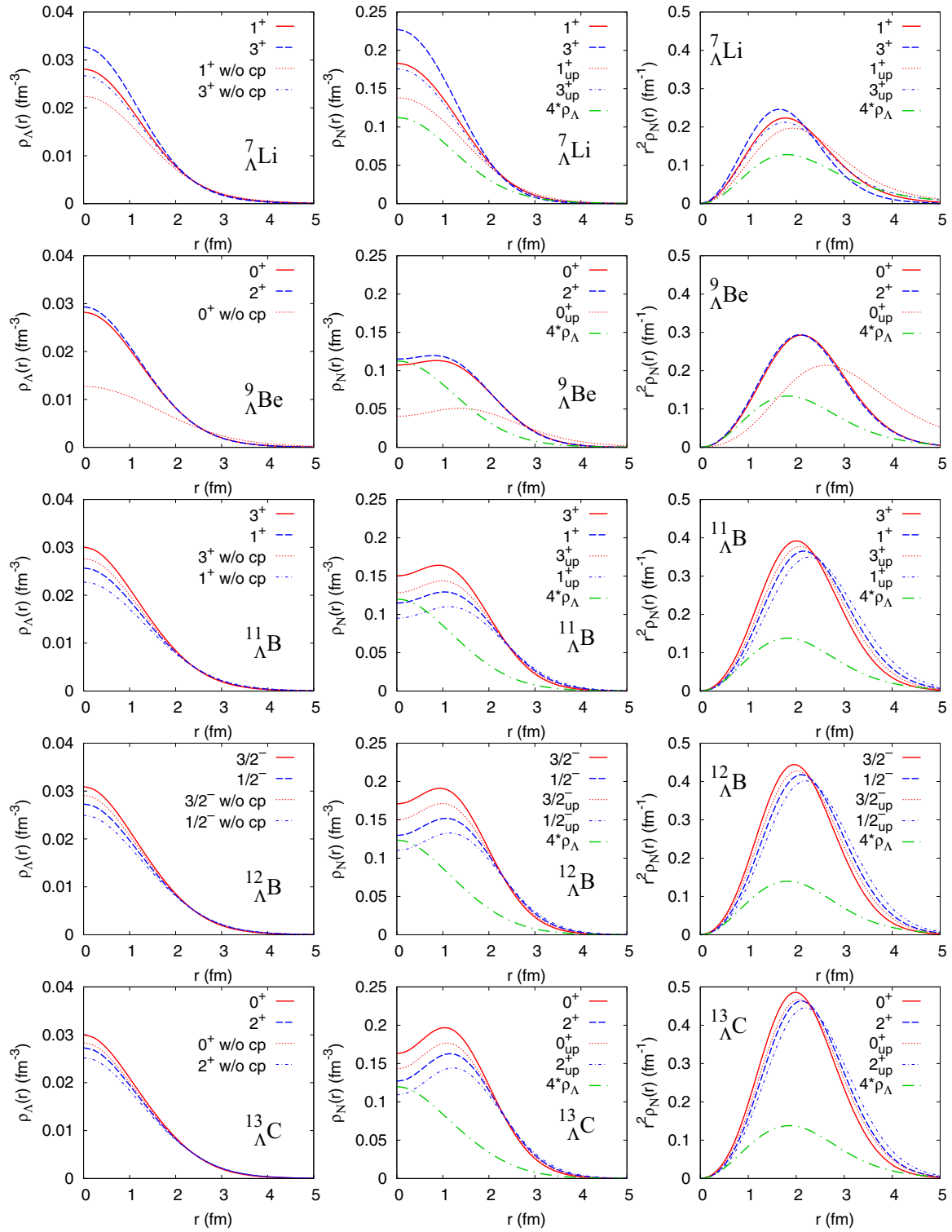


FIG. 4.  $\Lambda$  density and nuclear density distributions in  ${}^7_\Lambda\text{Li}$ ,  ${}^9_\Lambda\text{Be}$ ,  ${}^{11}_\Lambda\text{B}$ ,  ${}^{12}_\Lambda\text{B}$ , and  ${}^{13}_\Lambda\text{C}$  calculated with ESC08a(DI). In the left panels,  $\Lambda$  density obtained in the calculation with and without the core polarization (w/o cp) are shown. In the middle and right panels, nuclear densities and  $r^2$ -weighted densities are shown, respectively. In the middle panels,  $\Lambda$  density [ $\rho_\Lambda(r)$ ] multiplied by 4 in the ground state of  $A_\Lambda Z$  is also shown for comparison.

fm, and therefore, the  $\Lambda$  particle mainly probes the density difference between the ground and excited states in this region. Reflecting the nuclear density (size) difference between the

ground and excited states, the excitation energy shift occurs. The trend is similar in the results with and without the core polarization because the core polarization slightly raises the

inner nuclear density with almost the same amount in both ground and excited states.

### B. Size shrinkage in ${}^7_\Lambda\text{Li}$ and ${}^9_\Lambda\text{Be}$ : Comparison with other cluster model calculations

The shrinkage of cluster structures in  ${}^7_\Lambda\text{Li}$  and  ${}^9_\Lambda\text{Be}$  has been theoretically investigated in connection with  $\gamma$  transitions in details with the semimicroscopic  $\alpha + d + \Lambda$  and  $2\alpha + \Lambda$  cluster models, respectively, using the OCM [4,5]. The shrinkage and  $\gamma$  transitions in  ${}^7_\Lambda\text{Li}$  have been also investigated with the semimicroscopic  ${}^5_\Lambda\text{He} + p + n$  cluster OCM calculation [10]. The predicted size shrinkage in  ${}^7_\Lambda\text{Li}$  has been evidenced by the experimental measurement of the  $E2$  transition strengths for the  $5/2^+ \rightarrow 1/2^+$  transition [48].

I here describe the results for the shrinkage properties in  ${}^7_\Lambda\text{Li}$  and  ${}^9_\Lambda\text{Be}$ , and compare them with results of Refs. [4,10]. I also show comparison with the recent calculation of  ${}^9_\Lambda\text{Be}$  with a microscopic  $2\alpha + \Lambda$  cluster model with the  $S$ -wave  $\Lambda$  assumption in Ref. [19]. The interactions for the  $\Lambda$  particle in Ref. [4] are phenomenological  $\Lambda$ -cluster potentials, and those in Ref. [10] are the  $\Lambda$ -cluster potentials derived from the  $\Lambda NG$  interactions with phenomenologically adjusted  $k_f$  parameters. In Ref. [19], the density-independent  $\Lambda NG$  interactions with a fixed  $k_f$  parameter are used as the effective  $\Lambda$ - $N$  interactions. These effective interactions are state independent (structure independent) and, in that sense, they correspond to the density-independent treatment of  $k_f$  in ECS08a(DI) in the present calculation. For the results of Refs. [10,19], I show the values of the Nijmegen type-D (ND) case of the  $\Lambda NG$  parametrization.

In the works with semimicroscopic cluster models, the size shrinkage, i.e., the contraction of the  $\alpha + t$  and  $\alpha + \alpha$  cluster structures in  ${}^7_\Lambda\text{Li}$  and  ${}^9_\Lambda\text{Be}$  is usually discussed for the reduction of the rms distance between clusters because they are directly related to electric transition strengths in two-body cluster states. In particular, the  $E2$  transition strength from the  $D$ -wave excited state to the  $S$ -wave ground state is sensitive to the shrinkage because it is approximately proportional to the fourth power of the intercluster distance. To discuss the shrinkage of the cluster structures and its relation to the  $E2$  transitions, I approximately estimate the rms intercluster distances  $\bar{r}_{\alpha-x} \equiv \langle r_{\alpha-x}^2 \rangle^{1/2}$  between  $\alpha$  and  $x$  clusters from the calculated nuclear matter radius  $R_N$  using the following simple relation for nonmicroscopic two clusters,

$$(4 + A_x)R_N^2 = \frac{4A_x}{4 + A_x} \langle r_{\alpha-x}^2 \rangle + 4R_\alpha^2 + A_x R_x^2, \quad (43)$$

where  $x$  is  $d(\alpha)$  for  ${}^7_\Lambda\text{Li}({}^9_\Lambda\text{Be})$ , and  $A_x$  and  $R_x$  are the mass number and rms matter radius of the  $x$  cluster, respectively. I use the theoretical values  $R_\alpha = 1.55$  fm and  $R_d = 1.26$  fm for the  $(0s)^4$  and  $(0s)^2$  states with the present parametrization  $\nu = 0.235$  fm $^{-2}$ . I also approximate the  $\alpha$ - $\alpha$  distance  $\bar{r}_{\alpha-\alpha}$  in  ${}^9_\Lambda\text{Be}$  from  $R_N$  in Ref. [19] with (43) using their parameter  $\nu = 1/(2 \cdot 1.36^2)$  fm $^{-2}$ .

The size shrinkage in  ${}^7_\Lambda\text{Li}$  is characterized by the reduction of the distance  $\bar{r}_{\alpha-d}$  from  ${}^6\text{Li}$  to  ${}^7_\Lambda\text{Li}$ , and is discussed with the

TABLE VII.  $\alpha$ - $d$  distance  $\bar{r}_{\alpha-d}$  in  ${}^6\text{Li}$  and  ${}^7_\Lambda\text{Li}$ , and  $\Lambda$  binding energy ( $B_\Lambda$ ) and  $\Lambda$  distribution size ( $r_\Lambda$ ) in  ${}^7_\Lambda\text{Li}$  calculated with ESC08a(DI) and ESC08a(DD). The calculated  $B(E2; 3_1^+ \rightarrow 1_1^+)$  in  ${}^6\text{Li}$ ,  $B(E2; 3_1^+ \rightarrow 1_1^+, \text{core})$  in  ${}^7_\Lambda\text{Li}$ , the reduction factors  $S$  for the  $1_1^+$  and  $3_1^+$  states, and  $S_{E2}$  are also listed. Theoretical values of other calculations from Refs. [4,10], and experimental values from Refs. [48,66,70] are also listed. The  $\alpha$ - $d$  distance of Ref. [10] is the rms  $\alpha$ -( $pn$ ) distance.

|   | [4]  | [10] | present |      | exp      |
|---|------|------|---------|------|----------|
|   |      |      | DI      | DD   |          |
| ${}^6\text{Li}$                           |      |      |         |      |          |
| $\bar{r}_{\alpha-d}(1_1^+)$ (fm)          | 3.8  | 3.85 | 4.45    | 4.45 |          |
| $\bar{r}_{\alpha-d}(3_1^+)$ (fm)          | 3.66 |      | 4.16    | 4.16 |          |
| $B(E2)$ ( $e^2\text{fm}^4$ )              | 6.6  | 9.62 | 11.3    | 11.3 | 10.7(8)  |
| ${}^7_\Lambda\text{Li}$                   |      |      |         |      |          |
| $B_\Lambda$ (MeV)                         | 5.59 | 5.58 | 5.44    | 5.43 | 5.58(3)  |
| $\bar{r}_{\alpha-d}(1_1^+)$ (fm)          | 3.13 | 2.94 | 3.56    | 4.05 |          |
| $\bar{r}_{\alpha-d}(3_1^+)$ (fm)          | 2.91 |      | 3.02    | 3.56 |          |
| $r_\Lambda(1_1^+)$ (fm)                   | 2.4  |      | 2.57    | 2.66 |          |
| $r_\Lambda(3_1^+)$ (fm)                   | 2.33 |      | 2.42    | 2.61 |          |
| $B(E2, \text{core})$ ( $e^2\text{fm}^4$ ) | 3.2  | 3.1  | 3.4     | 6.2  | 4.6(1.3) |
| $S(1_1^+)$                                | 0.82 | 0.76 | 0.80    | 0.91 |          |
| $S(3_1^+)$                                | 0.80 |      | 0.72    | 0.86 |          |
| $S_{E2}$                                  | 0.83 | 0.75 | 0.74    | 0.86 | 0.81(4)  |

size reduction factor

$$S = \frac{\bar{r}_{\alpha-d}({}^7_\Lambda\text{Li})}{\bar{r}_{\alpha-d}({}^6\text{Li})}. \quad (44)$$

The reduction factor can be also reduced from the  $E2$  transition strengths for  ${}^6\text{Li}(3_1^+) \rightarrow {}^6\text{Li}(1_1^+)$  and  ${}^7_\Lambda\text{Li}(5/2^+) \rightarrow {}^7_\Lambda\text{Li}(1/2^+)$ , as

$$S_{E2} = \left[ \frac{B[E2; {}^6\text{Li}(3_1^+) \rightarrow {}^6\text{Li}(1_1^+)]}{(9/7)B[E2; {}^7_\Lambda\text{Li}(5/2^+) \rightarrow {}^7_\Lambda\text{Li}(1/2^+)]} \right]^{1/4}. \quad (45)$$

Here the denominator corresponds to the  $E2$  transition strength,  $B(E2; I_i^\pi \rightarrow I_f^\pi, \text{core})$ , for the  $3^+ \rightarrow 1^+$  transition of the core nuclear part in  ${}^7_\Lambda\text{Li}$ . The factor 9/7 is derived in the weak coupling limit of the core spin  $I$  and the  $\Lambda$  intrinsic spin [4].

Table VII shows the calculated results of the distance  $\bar{r}_{\alpha-d}$  in the ground and excited states of  ${}^6\text{Li}$  and  ${}^7_\Lambda\text{Li}$ ,  $B(E2)$  for  $3^+ \rightarrow 1^+$ , and the reduction factors compared with the theoretical values of Refs. [4,10]. For the  $B(E2; \text{core})$  values, the theoretical  $B(E2; 3^+ \rightarrow 1^+, \text{core}) = (9/7)B(E2; 5/2^+ \rightarrow 1/2^+)$  from Refs. [4,10] and the experimental value are shown. In the present calculation with ESC08a(DI), I obtain almost consistent results with those of other calculations. The distance  $\bar{r}_{\alpha-d}$  is significantly reduced in  ${}^7_\Lambda\text{Li}$  from  ${}^6\text{Li}$ . The reduction factor  $S_{E2}$  obtained with ESC08a(DI) agrees with the theoretical values of other calculations, and is in reasonable agreement with the experimental value within the error. In the ESC08a(DD) result, the size shrinkage is relatively small.



TABLE VIII.  $\alpha$ - $\alpha$  distance  $\bar{r}_{\alpha-\alpha}$  in  ${}^8\text{Be}$  and  ${}^9_\Lambda\text{Be}$ , and  $\Lambda$  binding energy ( $B_\Lambda$ ),  $\Lambda$  distribution size ( $r_\Lambda$ ), and  $B(E2; 2^+ \rightarrow 0^+, \text{core})$  in  ${}^9_\Lambda\text{Be}$  calculated with ESC08a(DI) and ESC08a(DD). Theoretical values of other calculations from Refs. [4,19] are also listed. The experimental  $B_\Lambda$  value is from Ref. [70].

|  | [4]  | [19] | present |      | exp     |
|--|------|------|---------|------|---------|
|  |      |      | DI      | DD   |         |
| ${}^8\text{Be}$                                  |      |      |         |      |         |
| $\bar{r}_{\alpha-\alpha}(0_1^+)$ (fm)            | 4.09 | 4.96 | 5.99    | 5.99 |         |
| ${}^9_\Lambda\text{Be}$                          |      |      |         |      |         |
| $B_\Lambda$ (MeV)                                | 7.49 | 7.33 | 7.04    | 6.43 | 6.71(4) |
| $\bar{r}_{\alpha-\alpha}(0_1^+)$ (fm)            | 3.46 | 3.61 | 3.76    | 4.41 |         |
| $\bar{r}_{\alpha-\alpha}(2_1^+)$ (fm)            | 3.44 | 3.56 | 3.71    | 4.65 |         |
| $r_\Lambda(0_1^+)$ (fm)                          | 2.39 | 2.57 | 2.44    | 2.67 |         |
| $r_\Lambda(2_1^+)$ (fm)                          | 2.39 | 2.55 | 2.41    | 2.67 |         |
| $B(E2, \text{core})$ ( $\text{e}^2\text{fm}^4$ ) | 11.3 | 13.1 | 15.2    | 31.6 |         |

Table VIII shows the results for  ${}^9_\Lambda\text{Be}$  with those of other calculations in Refs. [4,19]. Also for  ${}^9_\Lambda\text{Be}$ , the present calculation with ESC08a(DI) gives almost consistent results with those of Refs. [4,19]. The significant shrinkage occurs in  ${}^9_\Lambda\text{Be}$  as seen in the smaller  $\bar{r}_{\alpha-\alpha}$  value than that in  ${}^8\text{Be}$ .

### C. Interpretation of enhancement factor

In order to take into account the core polarization in  ${}^A_\Lambda Z$ , I add the artificial interactions  $\Delta H(\epsilon)$  to the Hamiltonian by slightly enhancing the central nuclear interactions. In the present cluster models, the perturbative interactions,  $\Delta H(\epsilon) = \epsilon V_N^{(c)}$ , act as slight enhancement of the intercluster potentials between inert clusters. It is consistent with the expectation from the glue-like role of a  $\Lambda$  particle. In a mean-field picture, this treatment corresponds to slight enhancement of the nuclear mean potentials  $U_N^{(NN)}(r) \rightarrow U_N^{(NN)}(r) + \epsilon U_N^{(NN)}(r)$  originating in the  $NN$  interactions. In a self-consistent mean-field approach, nucleons in  ${}^A_\Lambda Z$  feel the mean potentials  $U_N^{(NN)}(r) + U_N^{(\Lambda N)}(r)$ , where  $U_N^{(\Lambda N)}(r)$  is the  $\Lambda$ - $N$ -interaction-origin mean potentials for nucleons. In the case of  $\rho_\Lambda(r) \sim \rho_N(r)/(A-1)$  that the  $\Lambda$  distribution function is similar to the nuclear density distribution one,  $U_N^{(\Lambda N)}(r)$  may be approximated to be

$$\epsilon U_N^{(NN)}(r) \sim U_N^{(\Lambda N)}(r), \quad (46)$$

which corresponds to the present treatment of the core polarization. In the present results in  ${}^A_\Lambda Z$  in the  $6 < A < 14$  region, this condition is roughly satisfied as seen in the calculated  $\Lambda$  and nuclear densities as well as sizes  $r_\Lambda \sim R_N$ . Considering that  $U_N^{(\Lambda N)}(r) \sim U_\Lambda(r)/(A-1)$  in this condition, it leads to the relation,

$$\epsilon U_N^{(NN)}(r) \sim U_N^{(\Lambda N)}(r) \sim \frac{1}{A-1} U_\Lambda(r), \quad (47)$$

$$\epsilon \sim \frac{1}{A-1} \frac{U_\Lambda(r)}{U_N^{(NN)}(r)}. \quad (48)$$

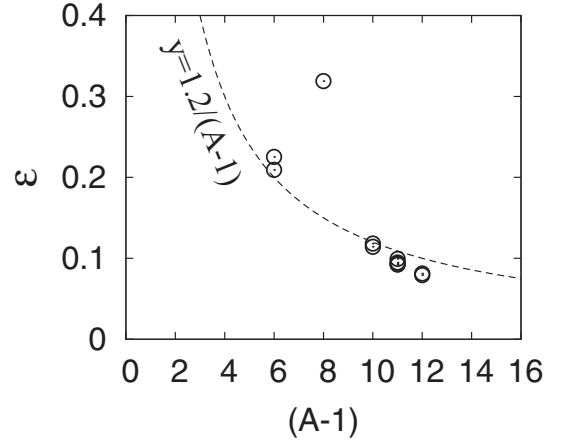


FIG. 5. Enhancement factor  $\epsilon$  in the ESC08a(DI) calculation. The factor is plotted as a function of  $A-1$ .

It means that the enhancement factor  $\epsilon$  can be proportional to  $1/(A-1)$ . Figure 5 shows the  $(A-1)$  dependence of the optimized  $\epsilon$  values, which are determined for each  ${}^A_\Lambda Z$  system to minimize the total energy. The  $\epsilon$  values are approximately on the  $1.2/(A-1)$  line except for  ${}^9_\Lambda\text{Be}$ , for which the mean-field picture may not work well because it is a dilute  $2\alpha$ -cluster system. The additional factor, 1.2, may come from various origins such as possible deviation from the relation  $\rho_\Lambda(r) \sim \rho_N(r)/(A-1)$ , the Pauli blocking between nucleons (no blocking between  $\Lambda$  and a nucleon), the weaker  $\Lambda$ - $N$  interactions than the  $N$ - $N$  interactions, and so on.

The picture discussed here may support the present treatment of the core polarization at least in the light mass-number region. However, it may not be obvious whether it is useful for heavier systems, in which the  $\Lambda$  particle is localized deeply inside the core nuclei and the condition  $\rho_\Lambda(r) \sim \rho_N(r)/(A-1)$  is no longer satisfied.

## VI. SUMMARY AND OUTLOOK

Structures of low-lying  $(0s)_\Lambda$  states in  $p$ -shell  $\Lambda$  hypernuclei were investigated with microscopic cluster models. To describe structures of the ground and excited states of core nuclei, I applied the GCM of microscopic  $\alpha + d$ ,  $2\alpha$ , and  $2\alpha + d$  cluster models for  ${}^6\text{Li}$ ,  ${}^8\text{Be}$ , and  ${}^{10}\text{B}$ , respectively, and that of  $2\alpha + t(h) + p_{3/2}$  and  $3\alpha + p_{3/2}$  models with the cluster breaking for  ${}^{11}\text{B}(\text{C})$  and  ${}^{12}\text{C}$ . The  $0s$ -orbit  $\Lambda$  particle in  $\Lambda$  hypernuclei is treated by the single  $S$ -wave channel calculation with the  $\Lambda$ -nucleus potentials, which are constructed by folding the effective  $\Lambda$ - $N$  interactions with the nuclear density obtained by the microscopic cluster models. As a core polarization effect, the core size reduction is taken into account in a simple way.

For  $A > 10$  systems, the core polarization, i.e., the nuclear size reduction by the  $\Lambda$  particle is small. The small change of the core size in the ground state of  ${}^{13}_\Lambda\text{C}$  is consistent with prediction of other calculations. Moreover, the core polarization effect on energy is minor and regarded as a higher-order perturbation in the  $\Lambda$  binding except for  $A < 10$ .

systems. However, it should be commented that the detailed energy balance between the nuclear energy increase and the  $\Lambda$  energy gain somewhat deviates from the ideal perturbative case meaning that a variational treatment of the core polarization is still necessary to discuss details of the size reduction in  $p$ -shell hypernuclei.

Energy spectra of the ground and low-lying excited states were discussed. Particular attention is paid to excitation energy shift and its relation to nuclear size difference between the ground and excited states in each  ${}^A_\Lambda Z$  system. The present results show a clear correlation between the energy shift and the size difference. Namely, the larger size difference, the larger excitation energy shift. The calculation with ESC08a(DI) qualitatively describes the systematic trend of the available experimental data for the energy shift. The mechanism of this correlation is understood as the higher nuclear density gives the larger attraction, i.e., the deeper  $\Lambda$ -nucleus potential. In other words, the  $0s$ -orbit  $\Lambda$  particle can probe the inner density difference through the  $\Lambda$ - $N$  interactions.

Shrinkage properties of the  $\alpha + d$  and  $2\alpha$  cluster structures in  ${}^7_\Lambda\text{Li}$  and  ${}^9_\Lambda\text{Be}$  were discussed, and the results were compared with those of other calculations. The obtained results are similar to those of other calculations. For  ${}^7_\Lambda\text{Li}$ , the results show the significant shrinkage, and reproduce the experimental  $E2$  transition strengths in  ${}^6\text{Li}$  and  ${}^7_\Lambda\text{Li}$  without using effective charges. Also in  ${}^9_\Lambda\text{Be}$ , the significant shrinkage occurs consistently with other calculations.

The effective  $\Lambda$ - $N$  interactions used in the present calculation are the spin-independent central interactions of the  $\Lambda NG$  interactions, which were derived from the  $\Lambda$ - $N$  interactions of the one-boson-exchange model based on the  $G$ -matrix calculation for an infinite nuclear matter. Two treatments and of the  $k_f$  parameter in the  $\Lambda NG$  interactions were adopted.

One is the density-independent (state-independent)  $\Lambda NG$  interactions and the other is the density-dependent (state-dependent)  $\Lambda NG$  interactions with the averaged density approximation. The present results indicate that the density-independent ESC08a interactions are rather favored in description of the systematic trend of experimental excitation energy shift in  ${}^A_\Lambda Z$  than the density-dependent ones. However, as for the quantitative reproduction, the density-independent calculation generally overestimates the experimental energy shift by a factor of 1.5–2. It is likely that weak density dependence of the  $\Lambda NG$  interactions may be suitable for detailed description of the excitation energy shift in  ${}^A_\Lambda Z$ . The density-dependent  $\Lambda NG$  interactions were constructed based on the  $G$ -matrix theory in an infinite nuclear matter and originally designed to reproduce systematics of  $\Lambda$  binding energy in  ${}^A_\Lambda Z$  in a wide mass-number region. The origin of the density dependence is the Pauli blocking effect on intermediate states in  $\Lambda$ - $N$  scattering processes. The Pauli suppression of the effective  $\Lambda$ - $N$  interactions is stronger in the higher nuclear density. However, it is not obvious that the density dependence of the  $\Lambda NG$  interactions can properly probe the density (or structure) difference between the ground and excited states in each  ${}^A_\Lambda Z$ . The present  $k_f$  dependence in the  $\Lambda NG$  interactions is likely to be too strong to simulate the structure

dependence of the effective interactions in low-lying states in each system.

One of the merits of the present calculation is that the framework is based on a microscopic calculation that can describe detailed nuclear structures such as energy spectra and cluster structures in  $p$ -shell nuclei. This is a great advantage for quantitative discussion of excitation energy shift by the  $\Lambda$  particle. Thanks to precise  $\gamma$ -ray measurements, there are many available data for energy spectra in  $p$ -shell hypernuclei, which enable one to finely tune the density dependence of the  $\Lambda$ - $N$  interactions by adjusting systematics of the excitation energy shift discussed in this paper.

The effect of density dependence of effective  $\Lambda$ - $N$  interactions on the core polarization in hypernuclei has been discussed with mean-field approaches using Skyrme parametrizations from the early days, for example, in Ref. [82]. It has been shown that density-independent  $\Lambda$ - $N$  interactions generally give large core polarizations whereas moderate density-dependent ones give less core polarization. The present result is qualitatively consistent with the mean-field analysis, but quantitatively, it shows significant size reduction in  $p$ -shell hypernuclei because the present model is able to describe large size reduction effects of cluster structures beyond mean-field approaches.

The present framework is based on local density approximations in treatment of nuclear density matrices of the exchange folding potentials and that of the density dependence of the  $\Lambda$ - $N$  interactions. The applicability of the present treatments to highly excited (particle-hole) states should be checked. In particular, the applicability to very dilute systems with much lower density than the saturation density should be carefully tested.

The present treatments of the  $\Lambda$  particle and the core polarization are very simple. However, one of the great advantages is that the method is handy and economical, and able to be applied to general nuclear structure models without changing computational codes for the nuclear structure calculation. Moreover, the method can be applied to double- $\Lambda$  hypernuclei straightforwardly.

In the present work, the spin-independent central  $\Lambda$ - $N$  interactions were used but spin dependence and the  $\Lambda$  spin coupling with the core nuclear spin were ignored. Within the present framework, it is able to discuss only the leading properties of energy spectra. In order to discuss detailed energy spectra and spin dependence of the  $\Lambda$ - $N$  interactions, some extensions of the framework are needed.

## ACKNOWLEDGMENTS

The author thanks to Dr. Motoba and Dr. Isaka for fruitful discussions. This work was inspired by the Karuizawa workshop (June 2017) and RCNP workshop (August 2017). The author would like to give a huge thanks to Dr. Fujiwara for his continuous encouragement. The computational calculations of this work were performed by using the supercomputer in the Yukawa Institute for theoretical physics, Kyoto University. This work was supported by JSPS KAKENHI Grant No. 26400270.

- [1] O. Hashimoto and H. Tamura, *Prog. Part. Nucl. Phys.* **57**, 564 (2006).
- [2] H. Tamura, *Prog. Theor. Phys. Suppl.* **185**, 315 (2010).
- [3] H. Tamura *et al.*, *Nucl. Phys. A* **914**, 99 (2013).
- [4] T. Motoba, H. Bandō, and K. Ikeda, *Prog. Theor. Phys.* **70**, 189 (1983).
- [5] T. Motoba, H. Bandō, K. Ikeda, and T. Yamada, *Prog. Theor. Phys. Suppl.* **81**, 42 (1985).
- [6] T. I. Yamada, K. Ikeda, H. Bando, and T. Motoba, *Prog. Theor. Phys.* **73**, 397 (1985).
- [7] Y. W. Yu, T. Motoba, and H. Bando, *Prog. Theor. Phys.* **76**, 861 (1986).
- [8] E. Hiyama, M. Kamimura, T. Motoba, T. Yamada, and Y. Yamamoto, *Phys. Rev. C* **53**, 2075 (1996).
- [9] E. Hiyama, M. Kamimura, T. Motoba, T. Yamada, and Y. Yamamoto, *Prog. Theor. Phys.* **97**, 881 (1997).
- [10] E. Hiyama, M. Kamimura, K. Miyazaki, and T. Motoba, *Phys. Rev. C* **59**, 2351 (1999).
- [11] E. Hiyama, M. Kamimura, T. Motoba, T. Yamada, and Y. Yamamoto, *Phys. Rev. C* **66**, 024007 (2002).
- [12] E. Hiyama, Y. Yamamoto, T. A. Rijken, and T. Motoba, *Phys. Rev. C* **74**, 054312 (2006).
- [13] E. Hiyama, T. Motoba, T. A. Rijken, and Y. Yamamoto, *Prog. Theor. Phys. Suppl.* **185**, 1 (2010).
- [14] E. Hiyama, M. Kamimura, T. Motoba, T. Yamada, and Y. Yamamoto, *Phys. Rev. Lett.* **85**, 270 (2000).
- [15] E. Cravo, A. C. Fonseca, and Y. Koike, *Phys. Rev. C* **66**, 014001 (2002).
- [16] V. M. Suslov, I. Filikhin, and B. Vlahovic, *J. Phys. G* **30**, 513 (2004).
- [17] M. Shoeb and Sonika, *Phys. Rev. C* **79**, 054321 (2009).
- [18] Y. Zhang, E. Hiyama, and Y. Yamamoto, *Nucl. Phys. A* **881**, 288 (2012).
- [19] Y. Funaki, T. Yamada, E. Hiyama, B. Zhou, and K. Ikeda, *Prog. Theor. Exp. Phys.* **2014**, 113D01 (2014).
- [20] Y. Funaki, M. Isaka, E. Hiyama, T. Yamada, and K. Ikeda, *Phys. Lett. B* **773**, 336 (2017).
- [21] A. Gal, J. M. Soper, and R. H. Dalitz, *Ann. Phys. (N.Y.)* **63**, 53 (1971).
- [22] A. Gal, J. M. Soper, and R. H. Dalitz, *Ann. Phys. (N.Y.)* **72**, 445 (1972).
- [23] A. Gal, J. M. Soper, and R. H. Dalitz, *Ann. Phys. (N.Y.)* **113**, 79 (1978).
- [24] D. J. Millener, *Nucl. Phys. A* **804**, 84 (2008).
- [25] D. J. Millener, *Nucl. Phys. A* **835**, 11 (2010).
- [26] D. J. Millener, *Nucl. Phys. A* **881**, 298 (2012).
- [27] N. Guleria, S. K. Dhiman, and R. Shyam, *Nucl. Phys. A* **886**, 71 (2012).
- [28] I. Vidana, A. Polls, A. Ramos, and H.-J. Schulze, *Phys. Rev. C* **64**, 044301 (2001).
- [29] X. R. Zhou, H.-J. Schulze, H. Sagawa, C. X. Wu., and E. G. Zhao, *Phys. Rev. C* **76**, 034312 (2007).
- [30] M. T. Win and K. Hagino, *Phys. Rev. C* **78**, 054311 (2008).
- [31] M. T. Win, K. Hagino, and T. Koike, *Phys. Rev. C* **83**, 014301 (2011).
- [32] B. N. Lu, E. G. Zhao, and S. G. Zhou, *Phys. Rev. C* **84**, 014328 (2011).
- [33] H. Mei, K. Hagino, J. M. Yao, and T. Motoba, *Phys. Rev. C* **90**, 064302 (2014).
- [34] H. Mei, K. Hagino, J. M. Yao, and T. Motoba, *Phys. Rev. C* **91**, 064305 (2015).
- [35] H. Mei, K. Hagino, J. M. Yao, and T. Motoba, *Phys. Rev. C* **93**, 044307 (2016).
- [36] H.-J. Schulze and E. Hiyama, *Phys. Rev. C* **90**, 047301 (2014).
- [37] M. Isaka, M. Kimura, A. Dote, and A. Ohnishi, *Phys. Rev. C* **83**, 044323 (2011).
- [38] M. Isaka and M. Kimura, *Phys. Rev. C* **92**, 044326 (2015).
- [39] H. Homma, M. Isaka, and M. Kimura, *Phys. Rev. C* **91**, 014314 (2015).
- [40] M. Isaka, Y. Yamamoto, and T. A. Rijken, *Phys. Rev. C* **94**, 044310 (2016).
- [41] M. Isaka, Y. Yamamoto, and T. A. Rijken, *Phys. Rev. C* **95**, 044308 (2017).
- [42] R. Wirth, D. Gazda, P. Navrátil, A. Calci, J. Langhammer, and R. Roth, *Phys. Rev. Lett.* **113**, 192502 (2014).
- [43] M. Isaka, M. Kimura, A. Dote, and A. Ohnishi, *Phys. Rev. C* **83**, 054304 (2011).
- [44] T. Sakuda and H. Bandō, *Prog. Theor. Phys.* **78**, 1317 (1987).
- [45] T. Yamada, K. Ikeda, H. Bandō, and T. Motoba, *Prog. Theor. Phys.* **71**, 985 (1984).
- [46] M. Isaka, H. Homma, M. Kimura, A. Dote, and A. Ohnishi, *Phys. Rev. C* **85**, 034303 (2012).
- [47] B. N. Lu, E. Hiyama, H. Sagawa, and S. G. Zhou, *Phys. Rev. C* **89**, 044307 (2014).
- [48] K. Tanida, H. Tamura, D. Abe, H. Akikawa, K. Araki, H. Bhang, T. Endo, Y. Fujii, T. Fukuda, O. Hashimoto, K. Imai, H. Hotchi, Y. Kakiguchi, J. H. Kim, Y. D. Kim, T. Miyoshi, T. Murakami, T. Nagae, H. Noumi, H. Outa, K. Ozawa, T. Saito, J. Sasao, Y. Sato, S. Satoh, R. I. Sawafuta, M. Sekimoto, T. Takahashi, L. Tang, H. H. Xia, S. H. Zhou, and L. H. Zhu, *Phys. Rev. Lett.* **86**, 1982 (2001).
- [49] D. L. Hill and J. A. Wheeler, *Phys. Rev.* **89**, 1102 (1953).
- [50] J. J. Griffin and J. A. Wheeler, *Phys. Rev.* **108**, 311 (1957).
- [51] D. M. Brink, *Proc. Int. School of Physics Enrico Fermi, Course 36, Varenna*, edited by C. Bloch (Academic Press, New York, 1966).
- [52] S. Saito, *Prog. Theor. Phys.* **41**, 705 (1969).
- [53] Y. Fujiwara *et al.*, *Prog. Theor. Phys. Suppl.* **68**, 29 (1980).
- [54] Y. Horiuchi, K. Ikeda, and H. Katō, *Prog. Theor. Phys. Suppl.* **192**, 1 (2012).
- [55] T. Suhara and Y. Kanada-En'yo, *Phys. Rev. C* **91**, 024315 (2015).
- [56] Y. Yamamoto, T. Motoba, and T. A. Rijken, *Prog. Theor. Phys. Suppl.* **185**, 72 (2010).
- [57] T. A. Rijken, M. M. Nagels, and Y. Yamamoto, *Prog. Theor. Phys. Suppl.* **185**, 14 (2010).
- [58] J. W. Negele and D. Vautherin, *Phys. Rev. C* **11**, 1031 (1975).
- [59] M. Kamimura, *Phys. Rev. A* **38**, 621 (1988).
- [60] E. Hiyama, Y. Kino, and M. Kamimura, *Prog. Part. Nucl. Phys.* **51**, 223 (2003).
- [61] A. B. Volkov, *Nucl. Phys.* **74**, 33 (1965).
- [62] N. Yamaguchi, T. Kasahara, S. Nagata, and Y. Akaishi, *Prog. Theor. Phys.* **62**, 1018 (1979); R. Tamagaki, *ibid.* **39**, 91 (1968).
- [63] E. Uegaki, S. Okabe, Y. Abe, and H. Tanaka, *Prog. Theor. Phys.* **57**, 1262 (1977).
- [64] E. Uegaki, Y. Abe, S. Okabe, and H. Tanaka, *Prog. Theor. Phys.* **62**, 1621 (1979).
- [65] F. Ajzenberg-Selove, *Nucl. Phys. A* **506**, 1 (1990).
- [66] D. R. Tilley, C. M. Cheves, J. L. Godwin, G. M. Hale, H. M. Hofmann, J. H. Kelley, C. G. Sheu, and H. R. Weller, *Nucl. Phys. A* **708**, 3 (2002).

- [67] D. R. Tilley, J. H. Kelley, J. L. Godwin, D. J. Millener, J. E. Purcell, C. G. Sheu, and H. R. Weller, *Nucl. Phys. A* **745**, 155 (2004).
- [68] J. H. Kelley, E. Kwan, J. E. Purcell, C. G. Sheu, and H. R. Weller, *Nucl. Phys. A* **880**, 88 (2012).
- [69] D. E. Lanskoy and Y. Yamamoto, *Phys. Rev. C* **55**, 2330 (1997).
- [70] D. H. Davis, *Nucl. Phys. A* **754**, 3 (2005).
- [71] M. Ukaï, S. Ajimura, H. Akikawa, D. E. Alburger, A. Banu, R. E. Chrien, G. B. Franklin, J. Franz, O. Hashimoto, T. Hayakawa, H. Hotchi, K. Imai, T. Kishimoto, M. May, D. J. Millener, S. Minami, Y. Miura, T. Miyoshi, K. Mizunuma, T. Nagae, S. N. Nakamura, K. Nakazawa, Y. Okayasu, P. Pile, B. P. Quinn, A. Rusek, Y. Sato, R. Sutter, H. Takahashi, L. Tang, H. Tamura, K. Tanida, L. Yuan, and S. H. Zhou (E930'01 Collaboration), *Phys. Rev. C* **73**, 012501 (2006).
- [72] H. Akikawa, S. Ajimura, R. E. Chrien, P. M. Eugenio, G. B. Franklin, J. Franz, L. Gang, K. Imai, P. Khaustov, M. May, P. H. Pile, B. Quinn, A. Rusek, J. Sasao, R. I. Sawafta, H. Schmitt, H. Tamura, L. Tang, K. Tanida, L. Yuan, S. H. Zhou, L. H. Zhu, and X. F. Zhu, *Phys. Rev. Lett.* **88**, 082501 (2002).
- [73] Y. Miura *et al.*, *Nucl. Phys. A* **754**, 75 (2005).
- [74] Y. Ma *et al.*, *Nucl. Phys. A* **835**, 422 (2010).
- [75] S. Ajimura, H. Hayakawa, T. Kishimoto, H. Kohri, K. Matsuoka, S. Minami, T. Mori, K. Morikubo, E. Saji, A. Sakaguchi, Y. Shimizu, M. Sumihama, R. E. Chrien, M. May, P. Pile, A. Rusek, R. Sutter, P. Eugenio, G. Franklin, P. Khaustov, K. Paschke, B. P. Quinn, R. A. Schumacher, J. Franz, T. Fukuda, H. Noumi, H. Outa, L. Gan, L. Tang, L. Yuan, J. Nakano, T. Tamagawa, K. Tanida, R. Sawafta, H. Tamura, and H. Akikawa (AGS-E929 Collaboration), *Phys. Rev. C* **65**, 034607 (2002).
- [76] H. Kohri, S. Ajimura, H. Hayakawa, T. Kishimoto, K. Matsuoka, S. Minami, Y. S. Miyake, T. Mori, K. Morikubo, E. Saji, A. Sakaguchi, Y. Shimizu, M. Sumihama, R. E. Chrien, M. May, P. Pile, A. Rusek, R. Sutter, P. M. Eugenio, G. Franklin, P. Khaustov, K. Paschke, B. P. Quinn, R. A. Schumacher, J. Franz, T. Fukuda, H. Noumi, H. Outa, L. Gan, L. Tang, L. Yuan, J. Nakano, T. Tamagawa, K. Tanida, R. Sawafta, H. Tamura, and H. Akikawa (AGS-E929 Collaboration), *Phys. Rev. C* **65**, 034607 (2002).
- [77] L. Tang *et al.* (HKS Collaboration), *Phys. Rev. C* **90**, 034320 (2014).
- [78] K. Hosomi *et al.*, *Prog. Theor. Exp. Phys.* **2015**, 081D01 (2015).
- [79] H. Morita and Y. Kanada-En'yo, *Prog. Theor. Exp. Phys.* **2016**, 103D02 (2016).
- [80] H. Morita and Y. Kanada-En'yo, *Phys. Rev. C* **96**, 044318 (2017).
- [81] M. Kamimura, *Nucl. Phys. A* **351**, 456 (1981).
- [82] M. Rayet, *Nucl. Phys. A* **367**, 381 (1981).